Environmental
Science
Advances

CRITICAL REVIEW
Quanguo He, Jun Liu *et al.*
Non-enzymatic electrochemical sensors based on
nanomaterials for detection of organophosphorus pesticide
residues

CRITICAL REVIEW

Check for updates

Non-enzymatic electrochemical sensors based on nanomaterials for detection of organophosphorus pesticide residues

Chuanqin Zhou, Jinxia Feng, Yaling Tian, Yiyong Wu, Quanguo He, [ID] * Guangli Li [ID] and Jun Liu*

Organophosphorus pesticides (OPPs) are one of the most popular pesticides. Once used, they inevitably affect the ecological chains and food chains of water, soil, and foodstuff sources, which can severely damage the ecosystem, and adversely affect human health. The shortcoming of enzymatic sensors, being the way in which enzymes are susceptible and vulnerable to environmental factors, could be compensated for, by using non-enzymatic nanosensors. Thus, it is important to develop effective non-enzymatic methods for the simple and fast analysis of the residues of OPPs. In order to develop new detection methods, a range of nanomaterials are being innovatively used to construct non-enzymatic electrochemical sensors endowed with specificity, selectivity, and cost-effectiveness. Herein, we review the latest research progress in the field of nano-materials and related composites used for the electrochemical non-enzymatic sensing of OPPs. The design method, detection limit, and sensing performances of both non-enzymatic nanomaterials and enzymatic ones were highlighted and compared. The challenges and prospects in this field are found and discussed. Undoubtedly, non-enzymatic sensors for OPP detection will facilitate the increasing demands of food and ecosystem monitoring and safeguarding.

Environmental significance

This article reviews the hazards of organophosphorus pesticides and the mechanisms of metabolism *in vivo* and in the environment. It summarizes and compares recent research advances in the field of nanomaterials and related composites for the electrochemical detection of organophosphorus pesticides, frequently used electrochemical detection mechanisms, the performance of electrochemical sensors, and the future prospects of non-enzymatic electrochemical detection.

1. Introduction

As we all know, pesticides are mainly used to control or eliminate pests, weeds, bacteria, rodents, and many other undesirable animals that do serious harm to modern agriculture. This is to improve the yield of crops.[1,2] However, only a small proportion of the pesticides are used up in the protection of the crops, with the rest being left in the ecological chain, or food chain, ending up in water, soil, and food. This severely damages the ecosystem and adversely affects human health and the environment.[3,4] Organophosphorus pesticides (OPPs) are derivatives of phosphoric acid, phosphonic acid, phosphinic acid, or phosphorothioate, usually in the form of esters, amides, or mercaptan-sulfur. Due to their features of strong insecticidal activity, short residual period, strong selectivity, high efficiency, and fast degradation, OPPs have become one of the most widely available pesticides in the world.[5,6] Generally speaking, the toxicity of OPPs can be broadly divided into three categories:

School of Life Sciences and Chemistry, Hunan University of Technology, Zhuzhou 412007, China. E-mail: zhouchuanqin0120@163.com; fengjinxia0828@163.com; tianyaling0212@163.com; wyy5082010@163.com; liu.jun.1015@163.com; guangli010@hut.edu.cn; hequanguo@hut.edu.cn; Fax: +86-731-22183383; Tel: +86-731-22183383

Chuanqin Zhou is a postgraduate student at the School of Life Sciences and Chemistry, Hunan University of Technology, China. Under the supervision of Professor Quanguo He, she is engaged in research on electrochemical detection.

Jinxia Feng is a postgraduate student at the School of Life Sciences and Chemistry, Hunan University of Technology, China. Under the supervision of Professor Quanguo He, she is engaged in research on electrochemical detection.

© 2023 The Author(s). Published by the Royal Society of Chemistry

Environ. Sci.: Adv., 2023, **2**, 933–956 | **933**

high toxicity, medium toxicity, and low toxicity. Excessive use of OPPs has affected crops and animals in various aquatic and terrestrial ecosystems. In particular, it may cause moderate toxicity in amphibians and fish (Fig. 1). The digestive tract, respiratory tract, skin, and mucous membranes are pathways for OPPs to enter the body. One of the main dangerous side effects of OPPs is the inhibition of acetylcholinesterase (AChE) activity in humans and animals, causing the accumulation of the neurotransmitter acetylcholine, and the stimulation of acetylcholine receptors. This can lead to many human diseases, such as contact dermatitis, respiratory difficulties, deformities, cancer, systemic paralysis, and even death.[7–12] According to data from the World Health Organization (WHO), there are 1500 million cases of diarrhea in children, caused by food and water pollution, every year, and more than 3 million deaths which are directly or indirectly caused by pesticide residues.

Like other organic compounds, OPPs undergo the processes of adsorption, volatilization, desorption, dissolution, hydrolysis, photodegradation, bioconcentration, and incomplete metabolism, if released into the environment. At present, OPPs in soil and water are mainly degraded by microorganisms, which means that pesticides are broken down into small inert products.[13] Different factors have certain impacts on the degradation rate, such as microbial composition, pH, temperature, and sunlight utilization rate.[14] However, the toxicity of some degradation products may be reduced, and others increased, owing to their incomplete degradation. For example, dibromophosphorus could be reduced by metal, to form the more toxic dichlorvos. Therefore, in order to use OPPs sensibly, many countries have stipulated maximum pesticide residue amounts in food and agricultural products.[15–17] The American Food and Drug Administration (FDA) has issued about 1045 maximum limits of pesticide residues. The European Community (EC) has published the Maximum Residue Limit (MRL) with respect to pesticides in food or feed. Canada and Japan have formulated their own limit standards. China has also formulated and introduced the national food safety standard 'Maximum Residue Limits of Pesticides in Foods GB 2763-2021' to replace the old standards and regulations. Compared with the previous standards, the new national standard has added and revised numerous pesticide residue limits, greatly increasing the coverage of pesticide residue limits. For example, the maximum residues of OPPs in citrus allowed by different countries have been summarized and listed in Table 1. As shown in Table 1, the EU has extremely strict limits for dimethoate, glufosinate-ammonium, and fenitrothion. This is due to the EU being the most strictly regulated pesticide region in the world, and the toxic side effects of these pesticides being relatively significant.

Although most of the pesticide residues in food testing are within the prescribed limits, when determined with specific detection methods, bioaccumulation inevitably leads to increased risks to human health. Thus, efficient approaches for analyzing the residues of OPPs are urgently needed to ensure food safety, protect ecosystems, and safeguard human health. At present, the conventional detection methods for OPPs include gas chromatography (GC),[18–21] high-performance liquid chromatography (HPLC),[22–26] gas chromatography-mass spectrometry (GC-MS),[27,28] enzyme-linked immunosorbent assay,[29–31] and so on. These methods can effectively detect different OPP compounds and residues, but there are disadvantages,

Yaling Tian is a postgraduate student at the School of Life Sciences and Chemistry, Hunan University of Technology, China. Under the supervision of Professor Quanguo He, she is engaged in research on electrochemical detection.

Yiyong Wu is a postgraduate student at the School of Life Sciences and Chemistry, Hunan University of Technology, China. Under the supervision of Professor Quanguo He, she is engaged in research on electrochemical detection.

Quanguo He was born in 1973. He obtained his MSc degree in Organic Chemistry from Xiangtan University in 2000, and his PhD degree in Biomedical Engineering from Southeast University in 2003, China. Then, he joined South China University of Technology as a postdoctoral researcher in 2005 and has been a professor at the Hunan University of Technology since 2008. He has been listed in the candidates of "Hunan Provincial 121 Talents Program" since 2010. His research interest covers biosensors, nanomaterials, and nano- & micro-devices. His recent research focus is on implant coating materials and ultrasensitive biochemical detection for various food and ecological chains. He has published more than 100 papers with total citations of more than 6500 in WOS.

Guangli Li is an associate professor at the School of Life Science and Chemistry, Hunan University of Technology, China. He received his PhD from the College of Chemistry and Molecules Sciences, Wuhan University, China in 2016 with the major of Physical Chemistry. Then, he joined the Hunan Key Laboratory of Biomedical Nanomaterials and Devices at Hunan University of Technology in 2017. He has presided over more than 10 research projects funded by the National Natural Science Foundation of China and other organizations. Additionally, he has published over 60 high-level academic papers in Journal of Hazardous Materials, Nanoscale, Sensors and Actuators B: Chemical, Journal of Neural Engineering, *and other similar ranked journals. His main research focuses on the development of advanced (bio)electrochemical sensors for biomedical and environmental applications and the design of novel biopotential electrodes for emerging wearable devices and real-life brain-computer interfaces.*

Jun Liu was born in 1988 and obtained his master's degree in biomedical engineering from Hunan University of Technology in 2014 and his PhD in materials physics and chemistry from Wuhan University in 2017. He has participated in several natural science foundation projects. He has published 30 papers in domestic and international academic journals.
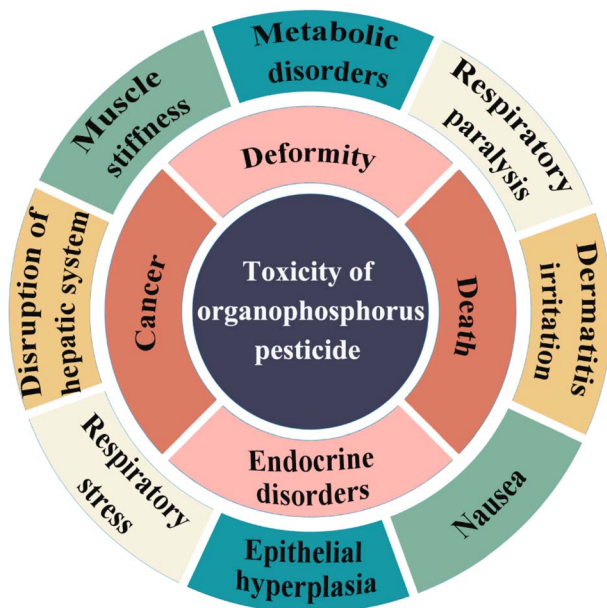
Fig. 1 Toxicity of organophosphorus pesticides to terrestrial and aquatic life.

commonly including complicated sample pretreatment and purification steps, and onerous requirements in technical personnel and equipment. These disadvantages restrict their practical use for fast and simple determination of OPPs. These newly emerging electrochemical sensors are considered to be more suitable means for the chemical analysis of OPPs, due to their greater convenience and improved availability.[32–36] Since OPPs can inhibit the activity of AChE, many enzymatic electrochemical sensors have been designed and developed based on the sensitivity of AChE to OPPs (the principle of the enzyme sensor is shown in Fig. 2). The AChE can catalyse acetylthiocholine chloride (ATCl), which produces thiocholine, an electroactive substance whose oxidation leads to an irreversible peak.[37,38] Sahub et al.[39] designed an enzyme-dependent luminescent biosensor for the detection of OPPs. Hydrogen peroxide from the enzymatic reactions of acetylcholinesterase and choline oxidase in this sensor could cause the graphene quantum dot fluorescence to be reduced, while OPPs weaken the enzymatic reactions and restore the fluorescence; Mahmoudi et al.[40] investigated an electrochemical biosensor with a modified metal–organic framework that introduced cerium (Ce) metal into the metal–organic framework, enhancing the loading site for acetylcholinesterase; and Yu et al.[41] fixed acetylcholinesterase on carbon nanotubes for the detection of OPPs. Experiments have shown that aminated carbon nanotubes have higher adsorption of enzymes and are more likely to promote enzymatic reactions. These enzyme-dependent sensors have good detection limits for OPPs. However, enzymes are usually affected by many uncontrollable environmental factors and are easily destroyed, making their use costly.

Recently, a variety of nanomaterials and composites with excellent electrochemical performance when combined with

Table 1 Different countries stipulate the maximum residue limit of OPPs in citrus[a]

OPPs	Structural formulas	U.S.	CODEX	EU	Canada	Korea	China
Dimethoate		2	5	0.01	1.5	2	2
Glufosinate-ammonium		0.15	0.05	0.05	0.1	0.05	0.5
Malathion		8	7	2	0.1	7	2
Chlorpyrifos		1	1	1.5	1	1	1
Phosmet		5	3	0.5	0.1	3	5
Fenitrothion		—	—	0.01	2	—	0.5

[a] The units are ppm. "–" indicates that the MRL of this pesticide in citrus is not specified.
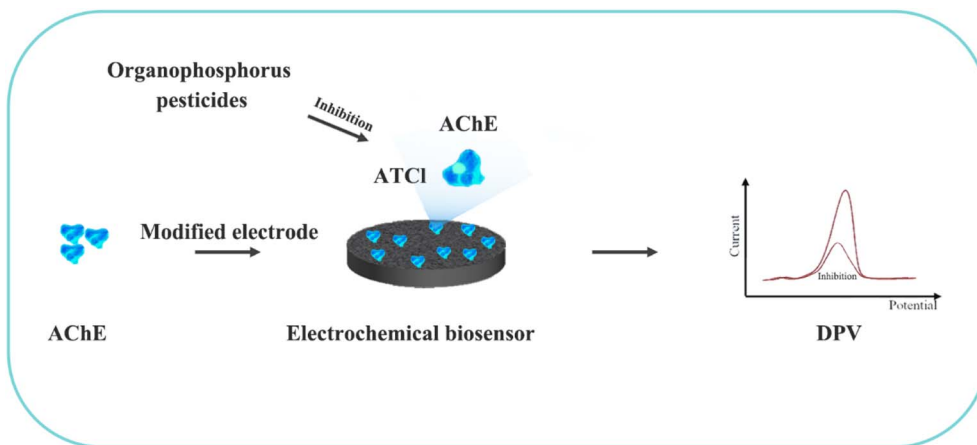
Fig. 2 The principle of the enzyme sensor.

metals, metal oxides, and polymers, to prepare non-enzymatic electrochemical sensors have been continuously reported by many researchers.[42–46] In this work, we have summarized the research progress of non-enzymatic carbon nanotubes, graphene, metal nanoparticles, metal oxides, conductive polymers, metal–organic frameworks and derivatives, molecularly imprinted polymers and their nanocomposite-modified electrodes, used in the electrochemical detection of OPPs (Fig. 3). Non-enzymatic sensors made from these materials offer simple fabrication, rapid processing, low technician and equipment requirements, and good anti-interference properties for the detection of OPPs in real samples. In addition, Table 2 shows the comparison with enzyme sensors, in which it can be seen that they have linear range and detection limits comparable to those of enzyme sensors, as well as superior stability. For example, the electrochemical sensor

BNQDs–GO/GCE (boron nitride quantum dots-graphene oxide/glassy carbon electrode) has a similar linear range to the biosensor AChE/Ce/UiO-66@MWCNTs/GCE (acetylcholinesterase/cerium/Zr-based MOFs/multi-walled carbon nanotubes) and shows a better detection limit and stability. Finally, we have discussed the problems and deficiencies that need to be considered in the construction of non-enzyme nanomaterials and modified electrodes. The challenges and prospects in this field are worth exploring further.

2. Toxicological effects of OPPs and their metabolism *in vivo* and in the environment

OPPs are heavily used because of their unique ability in improving crop yields and their relative environmental friendliness compared to organochlorine pesticides. However, their excessive use has had serious impacts on plants, animals, and the environment. Organophosphorus pesticide residues and their metabolites have been detected in humans, animals, plants, soil, and water sources, and have attracted widespread attention from scholars around the world.[47]

OPPs can inhibit the activity of a nervous system enzyme by a toxic mechanism that attacks the oxygen of the serine hydroxyl group at the active site of cholinesterase, causing the enzyme to be phosphorylated and thus inhibiting its physiological activity, leading to elevated levels of acetylcholine. This ultimately results in many pathologies.[48]

Most OPPs are phosphate esters or phosphorothioates. Their main structural type is shown in Fig. 4: "Z" is an oxygen or sulfur atom, such as parathion and paraoxon (the structural formula is shown in Table 2); "R_1" and "R_2" are mostly methoxy or ethoxy, such as fenitrothion and diazinon (the structural formula is shown in Table 2); and "X" is mostly alkoxy, aryloxy or others, such as fenamiphos and chlorpyrifos (the structural formula is shown in Table 2). Among them, OPPs with P=O functional groups are more toxic than those with P=S. The metabolism of OPPs in the body includes oxidation, hydrolysis, alkyl and aromatic transfer, reduction, and coupling. The enzymes that
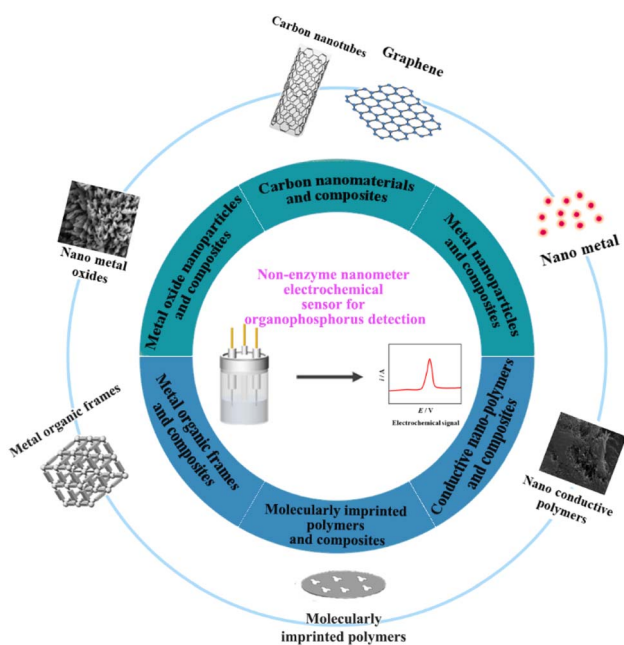

Fig. 3 Non-enzyme nanometer electrochemical sensor for organophosphorus detection.

Table 2 Comparison with enzymatic sensors

Electrode material	Detection method	Linear range (μM)	LOD (μM)	Accumulation/adsorption time	Stability	Anti-interference	Preparation difficulty level	OPPs	Ref.
GQDs/AChE/CHOx[a]	Luminescence	0.4–4.1	0.3	1800 s	N/A	Good	Difficult	Methyl paraoxon	39
AChE/Ce/UiO-66@MWCNTs/GCE[b]	DPV	1.0×10^{-6}–0.15	4.0×10^{-6}	720 s	Good	Good	Difficult	Paraoxon	40
AChE/CNT-NH$_2$/GCE[c]	DPV	2.0×10^{-4}–3.0×10^{-2}	8.0×10^{-5}	600 s	Good	Good	Difficult	Paraoxon	41
3DGH–AuNPs/APO/GCE[d]	DPV	1.0×10^{-5}–7.0×10^{-2}	3.5×10^{-6}	100 s	Excellent	Excellent	Normal	Diethylcyanophosphonate	92
BNQDs–GO/GCE[e]	DPV	1×10^{-6}–1.0×10^{-2}	3.1×10^{-4}; 6.7×10^{-8}; 3.3×10^{-8}	1800 s	Excellent	Excellent	Difficult	Parathion-methyl; diazinon; chlorpyrifos	93
PPy/Au-μE[f]	DPV	1.0×10^{-9}–1.0	0.9×10^{-9}	480 s	Excellent	Excellent	Normal	Chlorpyrifos	144

[a] Graphene quantum dots/acetylcholinesterase/choline oxidase. [b] Acetylcholinesterase/cerium/Zr-based MOFs/multi-walled carbon nanotubes. [c] Acetylcholinesterase/amino-functionalized carbon nanotubes/glassy carbon electrode. [d] 3D graphene-Au nanoparticles/4-aminoacetophenone oxime/glassy carbon electrode. [e] Boron nitride quantum dots-graphene oxide/glassy carbon electrode. [f] Polypyrrole/gold microelectrodes.

play these roles are CYPs (the cytochrome p450-dependent monooxygenase system), FMOs (the flavin-containing mono-oxygenases), esterases, glutathione transferases, glucuronosyltransferases, sulfotransferases and acetyltransferases.[49]

The initial metabolism of OPPs into the body is by CYP or FMO-mediated desulfurization and oxidation, a process in which the toxicity of OPPs is activated. For example, chlorpyrifos undergoes desulfurization by CYPs to produce chlorpyrifos-oxons that are thousands of times more toxic than themselves. In addition, a parallel and competing reaction to the desulfurization reaction is the dearylation, which is a CYP-mediated detoxification reaction. Another detoxification reaction mediated by CYPs is the dealkylation of OPPs, which leaves a monoalkyl phosphorothioate and aldehyde, and prevents subsequent desulfurization to achieve detoxification, such as the formation of monomethyl parathion and formaldehyde from methyl parathion. Besides, certain leaving groups of OPPs are sensitive to CYPs and can be subject to oxidation, after which they can be more easily involved in subsequent metabolism, such as hydroxylation, increasing their hydrophilicity and contributing to excretion. CYPs and FMOs can also mediate the sulfonation of the sulfur ether in phorate or phorate-oxon, which can be oxidized twice, the second oxidation from sulfoxide to sulfone only being able to be mediated by CYPs. This all increases the toxicity of the pesticide.[49,50]

2.1 Hydrolysis of OPPs *in vivo*

OPPs are extremely susceptible to hydrolysis by esterases, which is a detoxification process. The only insecticides or oxons that can be hydrolysed by A-esterases are those that have a P=O group in them. Thus, their ability to hydrolyse and detoxify phosphorothioate oxy-metabolites is a potentially important pathway for the detoxification of oxons, following CYP-mediated desulfurization to form oxons. Another relatively important hydrolytic enzyme is carboxylesterase. CarbEs (carboxylate esterase) can hydrolyse carboxylate esters such as in its hydrolysis of malathion, which is one of the most selective organophosphorus insecticides, as it is easily hydrolyzed by mammals but rarely by insects. CarbEs also has a detoxifying effect on many oxidants, this detoxification being saturable, such that if the concentration of OPPs is very high, its efficacy is limited.[50]

2.2 The next phase of metabolism

The biotransformations generated after pre-metabolism, where hydrophilic substituents are added to them so that they can be easily excreted, and their metabolites are detoxification products. For example, they are combined with glutathione and excreted intact from the bile by glutathione transferase, or converted to thiourea acid in the kidneys and hence excreted in the urine.[48–50]

Although the toxicity of the final products eliminated from the body is reduced, they may still be toxic, and in some cases may even induce a variety of diseases. In the environment, the metabolism of OPPs is primarily dependent on microbial decomposition, involving hydrolysis, oxidation, alkylation, and

© 2023 The Author(s). Published by the Royal Society of Chemistry

Environ. Sci.: Adv., 2023, **2**, 933–956 | **937**

dealkylation, which are enzymatic reactions in nature. However, the metabolism of microorganisms is long, the metabolic rate is low and the products of metabolism are still potentially harmful to the environment.[51]

3. Typical mechanisms involved in OPP electrochemical detection

Most OPPs are phosphate esters or phosphorothioates. There are two different categories of OPP detection methods, enzymatic and non-enzymatic. The enzymatic detection principle is based on the inhibition of cholinesterase by OPPs. Enzymatic-based sensors for OPP detection have been intensively investigated in recent years. However, the instability of enzymes limits their use. Compared to other methods for detecting OPPs, non-enzymatic electrochemical methods are simple, fast, sensitive, and selective. Currently, the typical mechanisms of non-enzymatic electrochemical sensors used to detect residues of OPPs are: direct electrochemical detection[52] and indirect electrochemical detection.[53,54]

Direct electrochemical detection means that the OPPs are directly detected by the redox reaction having an effect on electrode potential. For example, Wang et al.[56] designed graphene oxide dispersions modified with glassy carbon electrodes, to detect signals from the redox reaction of fenitrothion. OPPs are phosphate esters or phosphorothioates, and various types of direct electrochemical detection principles for OPPs are shown in Table 3. When the X-group (As shown in Fig. 3) of OPPs contains nitrogen or sulfur atoms, such as fenamiphos[42] and methyl parathion,[55] the redox reaction at these sites could be detected on electrochemical sensors, When the X-group contains the N (nitrogen) or C (carbon) double bond, such as diazinon[59] and dichlorvos,[62] the redox reaction at these sites could be detected on electrochemical sensors. In addition, in special environments, P=S groups could undergo desulfurization reactions, such as with malathion.[63]

Indirect electrochemical detection is the indirect detection of OPP concentrations by detecting other chemical/biological, energy, and signal transformations, under the influence of a working electrode. For example, Bakytkarim et al.[64] fabricated

a sensor modified with composite nanomaterials of silicon carbide and copper oxide, for the detection of malathion. The mechanism of the sensor is that CuO (copper oxide) exhibits excellent electrochemical behaviour in a blank buffer system, but when malathion is added to the solution, the electrochemical behaviour of CuO is inhibited, due to the high affinity of CuO for malathion, resulting in indirect detection of the amount of malathion. Furthermore, Kamyabi et al.[65] used ZnO (zinc oxide)/Ni-foam nanocomposites to construct an electrochemiluminescent sensor for the detection of chlorpyrifos. The principle behind this is that the disulfate anion is reduced and produces reactive radicals as SO_4^- radical sites, and ZnO is reduced at the negative potential, to produce anion radicals of $ZnO^{-\cdot}$. Then, the $SO_4^{-\cdot}$ radicals can interact with the $ZnO^{-\cdot}$ by injecting a hole into the valence band of ZnO and producing ZnO*. Finally, ZnO* generates a strong ECL signal.

4. Nonenzymatic nanomaterials for OPP detection

Nanomaterials have an increasing range of applications in electrochemical sensors and are a current research focus. Their excellent physical, chemical, and electrocatalytic properties could raise the performance of sensors to a new level. Nanomaterial-based non-enzymatic electrochemical sensors have the advantages of small size, simple operation, cost-effectiveness, high speed, and excellent sensitivity. Based on current research interests, nanomaterials used in non-enzymatic electrochemical sensors could be classified as carbon nanomaterials and composites, metal nanoparticles and composites, metal oxide nanoparticles and composites, conductive nano-polymers and composites, metal–organic frameworks and composites and molecularly imprinted polymers and composites. The types of nanomaterials include nanoparticles, nanotubes, nanowires, nanorods, nanofibres, nanofilms, and nanoblocks, which can be synthesized by gas-phase, liquid-phase, and solid-phase methods. Non-enzymatic sensors made from these materials offer simple fabrication, rapid processing, low technician and equipment requirements,
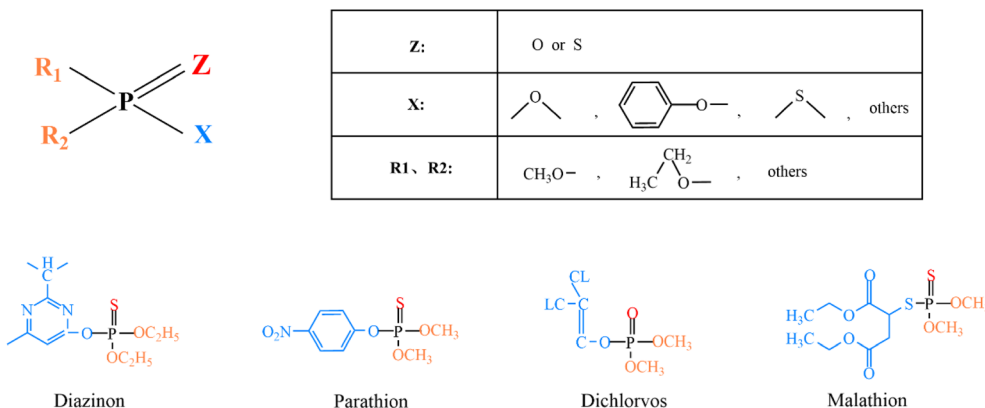

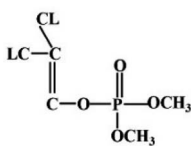**Fig. 4** Schematic diagram of the main type of OPP structure.
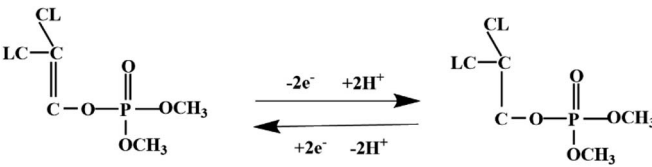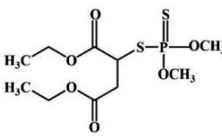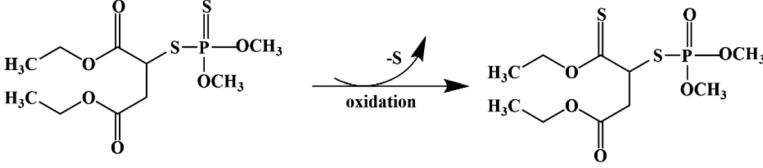
Table 3 Direct electrochemical detection of OPPs

OPPs	Structural formulas	Redox reaction		Ref.
Fenamiphos				42
Methyl parathion				55
Fenitrothion				56
Methyl paraoxon				57
4-Nitrophenyl phosphate				58
Diazinon				59
Phoxim				60
Chlorpyrifos				61

Table 3 (*Contd.*)

OPPs	Structural formulas	Redox reaction	Ref.
Dichlorvos	[structure of dichlorvos]	$\xrightarrow{-2e^-\ +2H^+}$ $\xleftarrow{+2e^-\ -2H^+}$	62
Malathion	[structure of malathion]	$\xrightarrow[\text{oxidation}]{-S}$	63

and good anti-interference properties for the detection of OPPs in real samples.

4.1 Carbon nanomaterials and composites

Carbon nanomaterials are one of the most widely used materials in electrochemistry, owing to their excellent structure, scalable performance, and remarkable abilities.[66–68] Various allotropes of carbon nanomaterials, such as carbon nanotubes (CNTs), graphene, and their derivatives are already being used as electrode materials for sensors.[69–74] Besides, the hidden potential applications of carbon nanomaterials and their composites in various fields are continually being found and exploited.[75–77] They have also been successfully used in the detection of OPPs. Different carbon nanomaterial electrocatalysts for the detection of OPPs are discussed in our work.

4.1.1 Graphene and composites. A novel material, graphene is a two-dimensional (2D) honeycomb lattice structure, in which carbon atoms linked by sp^2 hybrids are packed tightly into a single layer. It's able to fold into fullerenes, to roll into one-dimensional (1D) CNTs (carbon nanotubes), and to stack to obtain three-dimensional (3D) graphite. Due to its fast electron mobility, high surface area, remarkably high mechanical strength, stable chemical properties, and outstanding electrical conductivity, graphene has been utilized as an active catalytic material in fuel cells,[78] supercapacitors,[79,80] lithium-ion batteries[81,82] and solar cells.[83] In addition, there are applications of graphene oxide (GO), reduced graphene oxide (RGO), and functionalized graphene for the detection of numerous analytes in electrochemical sensors.[84–91]

Given the redox behavior of the OPP fenitrothion on the modified electrode, Wang *et al.*[56] established a new signal amplification electrochemical analysis method by modifying the GO on a glassy carbon electrode (GCE). The electrochemical reaction mechanism is that the nitrobenzene captures four electrons to form phenylhydroxylamine, resulting in an irreversible reduction peak. Then, a reversible peak is formed by the two-electron transfer between phenylhydroxylamine and nitrosobenzene. The porous structure of graphene oxide increases

the sensitivity of the electrode to signals. Wu *et al.*[92] constructed a diethyl cyanate sensor with a 3D graphene-Au nanoparticles/4-aminoacetophenone oxime (3DGH-AuNPs/APO) composite (Fig. 5). 3DGH-AuNPs were constructed by a straightforward one-pot hydrothermal method, in which hydroxylamine hydrochloride was used as the reducing agent, to obtain 4-aminoacetophenone oxime through an oximation reaction. 3D graphene can provide strong sites for AuNPs (Au nanoparticles), due to its high specific surface area and porous and fluffy structure, so that AuNPs can be distributed evenly. Additionally, AuNPs can not only greatly improve the conductivity of the sensor, but also serve as the binding site of 4-aminoacetophenone oxime.

Yola[93] proposed a new voltammetric sensor, fabricated with monodisperse boron nitride quantum dots (BNQDs) and GO, which was synthesized by a hydrothermal method, to simultaneously detect direct redox reactions with parathion-methyl, chlorpyrifos and diazinon in aqueous samples. The high surface area of GO creates more active sites at the surface of the electrode, enhancing the electrochemical response. Also, the synergistic effect between GO and BNQD increases the sensitivity to pesticide molecules, which further enhances the electrochemical activity of the electrode. Additionally, Rajaji *et al.*[94] designed a non-enzymatic electrochemical sensor for the detection of direct redox reactions of methyl paraoxon with 3D porous GO sheets coated chalcopyrite (copper iron(II) sulfide) (GOS@CuFeS$_2$). Bimetallic sulfide nanocomposites were used to build a fast and sensitive electrochemical sensor. The linear range was 0.073–801.5 μM, and the detection limit was 4.5 nM. Hashemi *et al.*[42] developed a new non-enzymatic electrochemical sensor to simultaneously detect two pesticides, consisting of reduced graphene oxide-Cu/CuO–Ag nanocomposites (rGO/Cu/CuO–Ag/GCE) modified on glassy carbon electrodes which exhibit excellent catalytic activity for the oxidation of carbaryl and fenamiphos pesticides. GO was synthesized by the modified Hummers' method and then dispersed in Cu/CuO–Ag solution to obtain rGO/Cu/CuO–Ag nanocomposites. Gao *et al.*[44] proposed that graphene nanosheets modified with gold and

940 | *Environ. Sci.: Adv.*, 2023, **2**, 933–956

© 2023 The Author(s). Published by the Royal Society of Chemistry

Fig. 5 Scheme of preparation for the 3DGH-AuNPs/APO/GCE electrochemical sensor and electrochemical detection of 4-amino-acetophenone oxime; TEM image of the 3DGH-AuNPs composite (A and B). Reproduced from ref. 92 with permission from Elsevier, copyright 2017.

zirconium oxide nanocomposites could be synthesized by a simple electrochemical co-deposition on glassy carbon electrodes (Au–ZrO$_2$-GNs/GCE) to detect methyl parathion, in which redox reactions occur. The strong affinity of zirconium oxide for phosphate groups and the remarkably high level of conductivity of graphene enabled the sensor to have excellent performance. Chen et al.[46] fabricated layered and porous three-dimensional structures of high-performance nitrogen-doped graphene (N-HG) electrochemical sensors which were synthesized by a hydrothermal method, to detect methyl parathion, by a redox reaction. The configuration of N bonds in N-HG was further investigated, and the results showed that pyrrolic-N has a crucial role in electrochemical processes and enhanced electrocatalysis.

4.1.2 Carbon nanotubes and composites. After the discovery of carbon nanotubes (CNTs) in 1991,[95] the excellent properties of CNTs in physical and chemical applications have received significant interest. A large number of studies on the synthesis, structure, and performance of CNTs have been conducted, which has promoted the advancement of CNTs. Normally, CNTs are categorized into two groups: single-walled carbon nanotubes (SWCNTs) and multi-walled carbon nanotubes (MWCNTs). There are several advantages of CNTs, including their high surface area, conductivity, mechanical resistance, variable surface chemistry, and their relative

chemical inertness in most electrolytes, which mean that CNTs can be broadly employed in the field of electrochemical sensors.[96–98]

Salehzadeh et al.[99] functionalized and dispersed CNTs in absolute ethanol to obtain CNTs with multiple hydroxyl groups, then modified them on a GCE to simultaneously determine the redox reactions of fenoxaphos and bifenox. The linear relationship was obtained in the range of 0.2–60 μM, and the detection limit was 0.08 μM. Despite CNTs showing excellent performance, the CNTs were often used in combination with other materials, like metallic nanoparticles and oxides, in previous studies. In the work of Dong et al.,[100] MWCNTs-cerium dioxide–Au nanocomposites (MWCNTs-CeO$_2$–Au) were obtained by the precipitation method and then used to detect p-sulfuric acid. The CeO$_2$ and AuNPs are uniformly distributed on the surface of MWCNTs. Compared to GCE and MWCNTs/GCE, MWCNTs-CeO$_2$–Au showed a significantly larger effective electrode surface area, which is mainly due to the increased specific surface area and volumetric ratio of CeO$_2$ and AuNPs decorated with MWCNTs. The specific surface area increase can improve the sensitivity of the detection, by enlarging the electrode reaction site, enhancing the adsorption capacity, and amplifying the current response of methyl parathion when redox reactions occur. The detection limit of methyl parathion was 0.0302 nM on the MWCNTs-CeO$_2$–Au/GCE.
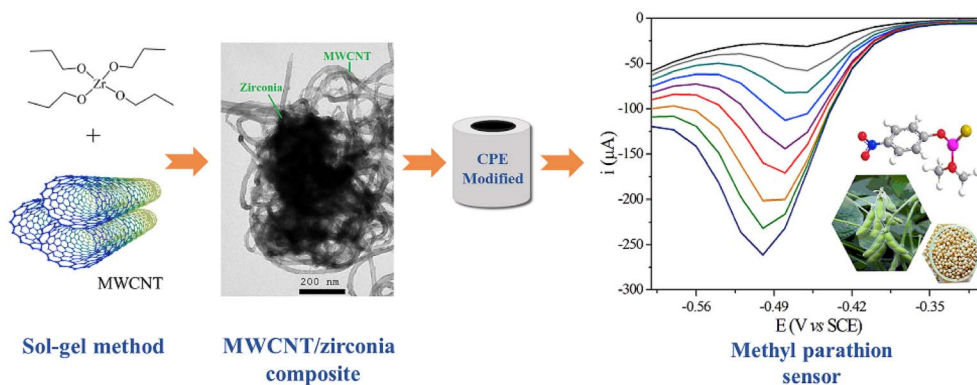
© 2023 The Author(s). Published by the Royal Society of Chemistry

Environ. Sci.: Adv., 2023, **2**, 933–956 | **941**

Fig. 6 Scheme of preparation for the MWCNT/ZrO$_2$/CPE electrochemical sensor and electrochemical detection of methyl parathion. Reproduced from ref. 101 with permission from Elsevier, copyright 2020.

Additionally, Huo *et al.*[69] developed a novel sensor for malathion determination with a composite composed of SWCNTs and CuO nanowires (CuO NWs), which were prepared by thermal oxidation. The strong adsorption force between the SWCNTs with a network structure and the malathion, and the good affinity between CuO NWs and malathion, allow the indirect detection of malaprop by enhanced electron transfer capacity. Thereby, the improved performance and good stability of CuO NWs–SWCNTs serve as the basis for the electrochemical quantification of malathion. Ghodsi *et al.*[59] developed a sensor with MWCNTs/TiO$_2$ (titanium dioxide) NPs to detect diazinon based on diazinon reduction. MWCNTs/TiO$_2$NPs, synthesized by the calcination method were employed successfully to the determination of diazinon in actual samples, which can be ascribed to their excellent synergistic electrocatalytic performance. Dos Santos Caetano *et al.*[101] dispersed multi-walled carbon nanotubes (MWCNT) in a zirconia matrix, synthesized by the sol–gel method for the detection of methyl parathion, by a redox reaction (Fig. 6). The MWCNT/ZrO$_2$ (zirconium dioxide) nanocomposite has a multiporous structure and its modified carbon paste electrode has excellent performance.

In summary, carbon nanomaterials have the benefits of significant specific surface area, simple synthesis methods, and good catalytic capability. Generally, the high specific surface area of carbon nanomaterials is used to enhance the strong adsorption of the target analyte, and the improved electrochemical reaction signal, by using the affinity of their surface for the target analyte to enhance electron transfer. Furthermore, compared with carbon nanomaterials that work alone, the combination of other conductive materials with carbon nanocomposites can produce synergistic effects, which can enhance the reaction sites and the electron transfer rate, to obtain better results. The relevant data of electrochemical sensors for detection of different OPPs using graphene and carbon nanotube composites are listed in Table 4. Graphene and carbon nanotube composites have an obvious detection ability for OPPs. It is worth noting that the composite material of GO and BNQDs forms a specific and sensitive pesticide molecular cavity, resulting in a lower LOD, which can reach the ppm range. The maximum allowable residues of diazinon and chlorpyrifos in

vegetables and crops are 0.1 ppm and 1 ppm in China. BNQDs–GO/GCE is expected to become a convenient method to analyze actual samples in the future. A large amount of data indicate that composite materials are more conducive to the electrochemical detection of pesticides. Therefore, we hope to develop more carbon nanomaterials and composites, to fabricate OPP electrochemical sensors with simple preparation processes and excellent performance. The commercialization of convenient and fast micro-sensors will also be a direction of future development.

4.2 Metal nanoparticles and composites

The development of electrochemical sensors based on metal nanoparticles (NPs) has always been a hot topic. Generally speaking, sensors prepared from metal NPs have a host of advantages, such as large specific surface area, fast electron transfer, and mass transfer speed. Besides, they can also improve analysis parameters, such as detection limit, sensitivity, stability, and multiple detection capabilities. Among the existing metal NPs, AuNPs have made a great contribution to sensors used in the environment, a fact attributable to their fine optical properties, high surface area, and surface modification capabilities. They have been employed as an effective electrocatalyst in many electrochemical reactions, because they are stable and can be reused in the redox process. With these remarkable characteristics, electrochemical sensors fabricated with metal NPs and their composites, for the detection of OPP pesticides, are summarized in this work.

In the work of Gao *et al.*,[102] nanoporous gold (NPG) was fabricated by chemical corrosion of the Au/Ag binary alloy in concentrated HNO$_3$ for GCE modification. Then, NPG/GCE was constructed to directly detect methyl parathion and carbendazim simultaneously, using NPG as the active electrocatalyst. During the dealloying process, when the Au/Ag alloy was immersed in concentrated HNO$_3$ (nitric acid), the active Ag atoms in the alloy were removed, and the remaining inert Au atoms self-assembled into an open continuous 3D sponge-like structure. Moreover, the thickness of the AuNP film is about 100 nm, making it easy to combine with the GCE. CV and DPV were utilized to study the electrochemical properties of NPG/

Table 4 Comparison of electrochemical properties of carbon nanomaterials and their composite modified electrodes for OPP determination

Electrode material	Detection method	Linear range (μM)	LOD (μM)	Accumulation/adsorption time	Stability	Anti-interference	Preparation difficulty level	OPPs	Ref.
rGO/Cu/CuO–Ag/GCE[a]	DPV	5.0×10^{-2} – 20.0	3.0×10^{-3}	N/A	Average	Good	Normal	Fenamiphos	42
Au–ZrO$_2$-GNs/GCE[b]	SWV	3.8×10^{-3}-9.1	3.8×10^{-3}	720 s	Good	Good	Normal	Methyl parathion	44
N-HG$_{50}$/GCE[c]	DPV	3.8×10^{-3}-570	1.3×10^{-5}	N/A	Good	Excellent	Normal	Methyl parathion	46
GO/GCE[d]	SWV	3.6×10^{-3}-1.4	3.6×10^{-4}	120 s + 240 s	Average	Good	Easy	Fenitrothion	56
MWCNTs/TiO$_2$NPs/GCE[e]	SWV	1.1×10^{-2}-8.4	3.0×10^{-3}	5 s	Good	N/A	Normal	Diazinon	59
SWCNTs-CuO NWs/GCE[f]	DPV	0–0.6	3.0×10^{-4}	160 s	Excellent	Excellent	Normal	Malathion	69
3DGH-AuNPs/APO/GCE[g]	DPV	1.0×10^{-5}–7.0×10^{-2}	3.5×10^{-6}	100 s	Excellent	Excellent	Normal	Diethylcyano-phosphonate	92
BNQDs–GO/GCE[h]	DPV	1×10^{-6}-0.01	3.1×10^{-4}; 6.7×10^{-8}; 3.3×10^{-8}	1800 s	Excellent	Excellent	Difficult	Parathion-methyl; diazinon; chlorpyrifos	93
GOS@CuFeS$_2$/GCE[i]	DPV	7.3×10^{-2}-801.5	4.5×10^{-3}	N/A	Good	Excellent	Normal	Methyl paraoxon	94
MWCNTs/GCE[j]	SWV	0.2–60.0	8.0×10^{-2}	90 s	N/A	Excellent	Easy	Fenitrothion	99
MWCNTs-CeO$_2$–Au/GCE[k]	DPV	1.0×10^{-4}-0.1	3.0×10^{-5}	N/A	Excellent	N/A	Normal	Parathion-methyl	100
MWCNT/ZrO$_2$/CPE[l]	DPV	176.8–19.9×10^6	9.0×10^{-3}	15 s + 60 s	N/A	Good	Normal	Methyl paraoxon	101
Pd/MWCNTs/GCE[m]	DPV	0.4–53.2	0.2	N/A	Excellent	Good	Normal	Methyl parathion	105

[a] Reduced graphene oxide-Cu/CuO–Ag nanocomposite/glassy carbon electrode. [b] Gold–zirconia nanocomposites/graphene nanosheets/glassy carbon electrode. [c] Nitrogen-doped holey graphene/glassy carbon electrode. [d] Graphene oxide/glassy carbon electrode. [e] Multiwalled carbon nanotubes/TiO$_2$ nanoparticles/glassy carbon electrode. [f] Single carbon nanotubes–CuO nanowires/glassy carbon electrode. [g] 3D graphene-Au nanoparticles/4-aminoacetophenone oxime/glassy carbon electrode. [h] Boron nitride quantum dots-graphene oxide/glassy carbon electrode. [i] 3D porous graphene oxide coated chalcopyrite/glassy carbon electrode. [j] Multiwalled carbon nanotubes/glassy carbon electrode. [k] Multiwalled carbon nanotubes–CeO$_2$–Au/glassy carbon electrode. [l] Multiwalled carbon nanotubes/zirconia/carbon paste electrode. [m] Palladium/multiwalled carbon nanotubes/glassy carbon electrode.

GCE in relation to methyl parathion and carbendazim. It was found that AuNPs/GCE has good selectivity and anti-interference ability. The detection limits of methyl parathion and carbendazim were 0.02 μM and 0.24 μM, respectively. Balasubramanian et al.[57] adopted tannin as a bifunctional green reducing and stabilizing agent, to obtain tannic acid-coated AuNPs (TA@AuNPs) for the direct detection of methyl parathion, following a simple classical nucleation and growth mechanism. TA@AuNPs show a stronger affinity for methyl parathion than metal ions and other nitroaromatic compounds. Yan et al.[62] detected dichlorvos by covalently attaching AuNPs and RGO to polyamine-based ferrocene dendrimer (FcDr) (Fig. 7). Dichlorvos can be absorbed by electrostatic action onto the FcDr/rGO surface and then react with FcDr, leading to a redox signal. In the work, the dendrimer FcDr has a natural redox signal center (Fe^{3+}/Fe^{2+}), which can provide a large amount of active termini of carboxyl groups and a compact matrix for the covalent connection of RGO and AuNPs. The purpose of using RGO nanosheets with larger surface areas is that more AuNPs with superior electrical conductivity and catalytic activity can be deposited on their surface. Together, AuNPs and rGO nanosheets can accelerate the electron transfer from FcDr to the glassy carbon electrode (GCE), resulting in amplified electrochemical signals from AuNPs/FcDr/rGO/GCE

sensors. Gong et al.[103] chose chitosan as a stabilizer, to prepare a chitosan-graphene solution, in order to prevent graphene from forming irreversible agglomerates. AuNPs were deposited at the chitosan-graphene-modified electrode surface, and the AuNPs-chitosan-graphene modified electrode (AuNPs-chi-GNs/GCE) was prepared. The sensor promotes the enrichment of nitroaromatic chemicals. Methyl parathion was enriched on AuNPs-chi-GNs/GCE, resulting in a redox reaction.

PdNPs (palladium nanoparticles) also show high electrocatalytic activity for various analytes, and the cost of Pd (palladium) is relatively low compared to Au and Pt, which means that Pd is a suitable alternative in an electrochemical sensor. Thus, a great number of studies for OPP determination based on PdNPs and their composites have been reported. Renganathan et al.[104] fabricated PdNPs/boron nitride heterojunctions (PdNPs/BN HJs) using sonochemical methods, for paraoxon ethyl detection, in which the nitro group is converted to phenylhydroxylamine. During the synthesis process, BN was functionalized with hydroquinone (HQ) and acted as a reducing agent for PdNPs. The obtained PdNPs/BN HJs have significant electrocatalytic performance for paraoxon, which is ascribed to the large surface area of the BN HJs, the good conductivity of PdNPs, and their synergy. Huang et al.[105] prepared Pd/MWCNTs in ethylene glycol (EG) solution by a reduction method. The Pd/

MWCNTs/GCE sensor was used to detect methyl parathion. Through the electrochemical behavior of methyl parathion on Pd/MWCNTs/GCE, it was found that PdNPs have the characteristics of reversible hydrogen adsorption and desorption. Both the H^+ involved in the reaction and the large surface area of Pd/MWCNT are beneficial to the adsorption and reduction of methyl parathion. Additionally, Sreedhar *et al.*[106] used composites with Ag/Cu alloy nanoparticles and graphene to increase the electron transfer rate and electrical conductivity of the sensor, to detect chlorpyrifos through the reductive cleavage of the C–Cl (carbon–chlorine) bond. The sensor mixes Ag/Cu alloy nanoparticles, graphene, and mineral oil at a ratio of 65/5/30 (w/w) %. Bimetallic nanoparticles combined with graphene increase the stability, catalytic activity, and active sites of the electrode.

In Table 5, the analysis parameters of non-enzyme catalyzed OPP sensors based on precious metal and bimetal nanocomposite were compared. Metal NPs play an important role in the electrochemical detection of OPPs. Metal NPs with a common structure usually have high conductivity and fast electron transferability, while metal nanoparticles with 3D or porous structures can provide a larger surface area for combining with other materials. It is because of these advantages that electrochemical sensors based on metal nanoparticles can achieve lower detection limits. Take the electrochemical detection of parathion-methyl as an example, the lowest detection limit can reach the nm range with AuNP and PdNP composites. However the detection limit of parathion-methyl determined by the GC in the Chinese national standard 'GB/T 5009.20-2003' can reach the ppm level.
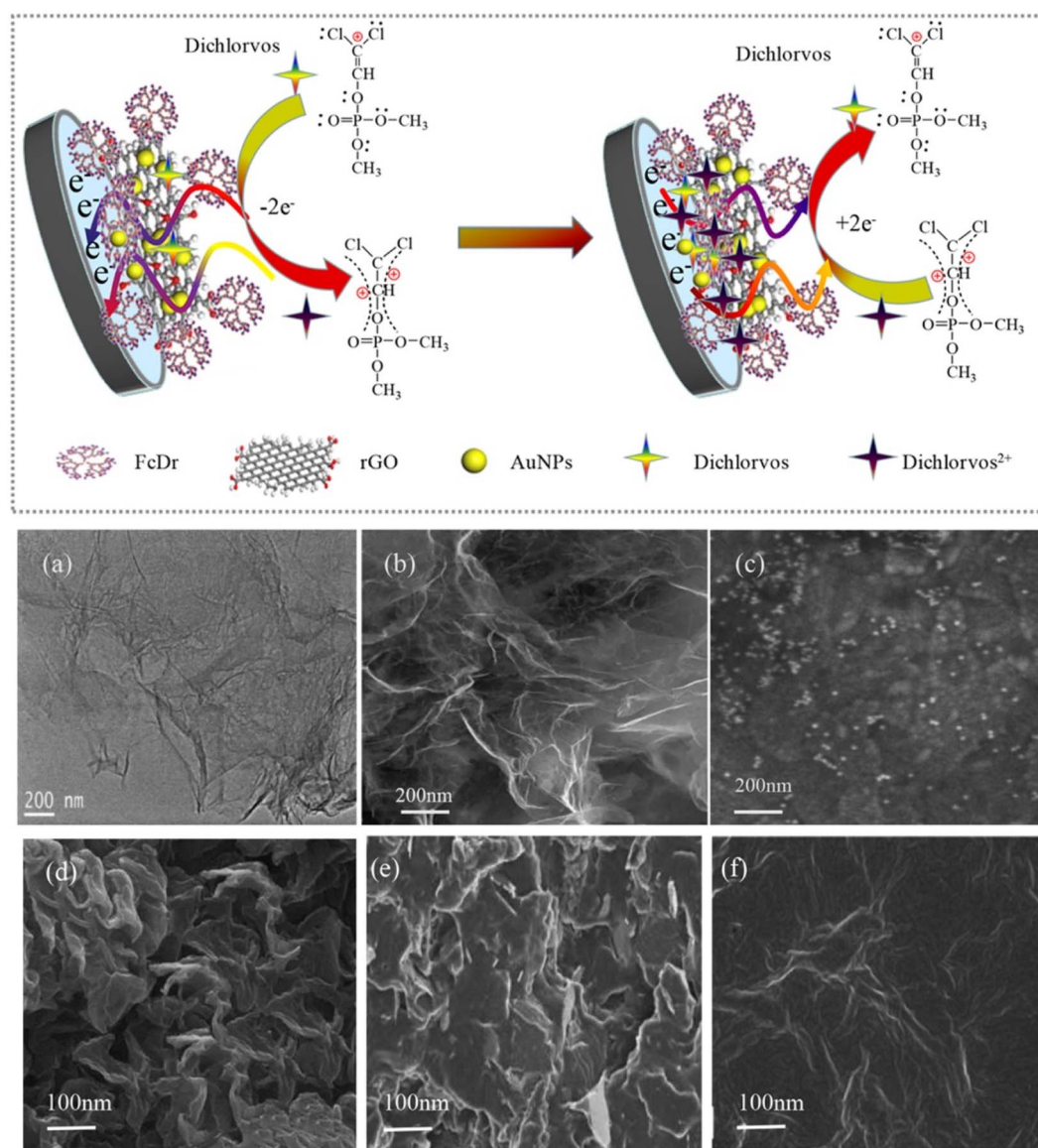

Fig. 7 Scheme of the AuNPs/FcDr/RGO/GCE electrochemical sensor to detect dichlorvos, SEM images of rGO nanosheet (a), FcDr/rGO (b) and AuNPs/FcDr/rGO (c), and SEM images of rGO/GCE (d), monolayered Au/FcDr/rGO/GCE (e), and double layered Au/FcDr/rGO/GCE (f). Reproduced from ref. 62 with permission from Elsevier, copyright 2020.

Table 5 Comparison of electrochemical properties of nano-metal particles and their composite modified electrodes for OPP determination

Electrode material	Detection method	Linear range (μM)	LOD (μM)	Accumulation/ adsorption time	Stability	Anti-interference	Preparation difficulty level	OPPs	Ref.
TA@AuNPs/GCE[a]	DPV	3.3×10^{-2}–167.7	1.1×10^{-4}	150 s	Good	Excellent	Easy	Methyl paraoxon	57
CoNPs/PPy/GCE[b]	SWV	2.5×10^{-2}–12.0	4.5×10^{-3}	50 s	Average	Excellent	Normal	Phoxim	60
AuNPs/FcDr/RGO/GCE[c]	DPV	0.4–218.4	0.2	1.8 s	Excellent	Good	Difficult	Dichlorvos	62
NPG/GCE[d]	DPV	0.5–150	2.0×10^{-2}	N/A	N/A	Excellent	Easy	Methyl paraoxon	102
AuNPs-chi-GNs/GCE[e]	SWV	3.8×10^{-3}–0.4; 0.8–3.8	2.3×10^{-3}	1200 s	N/A	Excellent	Normal	Methyl paraoxon	103
PdNPs/BN HJ/GCE[f]	LSV	9.0×10^{-2}–210.0	5.0×10^{-3}	N/A	N/A	Excellent	Easy	Methyl paraoxon	104
Pd/MWCNTs/GCE[g]	DPV	0.4–53.2	0.2	N/A	Excellent	Good	Normal	Methyl paraoxon	105
Ag/Cu–GRPE[h]	DPV	0.1×10^{-4}–0.1	4.0×10^{-6}	120 s	Excellent	Excellent	Easy	Chlorpyrifos	106
CuNPs@GR-MIP[i]	DPV	5.0×10^{-2}–50.0	0.2×10^{-3}	720 s	Excellent	Excellent	Normal	Parathion methyl	149

[a] Tannic acid-coated AuNPs/glassy carbon electrode. [b] Cobalt nanoparticles/polypyrrole/glassy carbon electrode. [c] AuNPs/dendrimer/reduced graphene oxide/glassy carbon electrode. [d] Nanoporous Au/glassy carbon electrode. [e] AuNPs-chitosan-graphene/glassy carbon electrode. [f] PdNPs/BN heterojunctions/glassy carbon electrode. [g] Pd/multi-walled carbon nanotubes/glassy carbon electrode. [h] Ag/Cu alloy nanoparticles/graphene nanocomposite paste electrode. [i] Copper nanoparticle-decorated vinyl-functionalized graphene/glassy carbon electrode.

Therefore, electrochemical sensor materials with better performance and lower cost will need to be developed in the future.

4.3 Metal oxide nanoparticles and composites

Although noble metals are ideal materials for constructing non-enzymatic OPP sensors, the application is greatly restricted, owing to their high cost. Metal oxides, as a cost-effective choice, are usually combined with conductive materials, such as 3D graphene, MWCNTs, and organometallic frameworks, to improve their conductivity and form layered nanostructures with large surface areas and more active sites. Using different preparation methods, metal oxides can be made into different shapes (tubes, fibers, threads, needles, rods, and balls) and give them various properties. Therefore, various electrochemical sensors can be prepared, as required.

In recent reports, nano CuO has been used for OPP detection because it can bind with the phosphate groups in OPPs. CuO with a large surface area and active sites, excellent redox performance, and chemical stability, is considered a promising material. However, due to poor electrical conductivity, CuO is often compounded with other conductive materials. Xie et al.[53] synthesized 3D graphene (3DGR) by a hydrothermal method. The three-dimensional graphene framework provides a large surface area for the dispersion of CuO-NPs and also improves the conductivity of the electrodes. As the result of the electrochemical behavior indicated, the specific adsorption of malathion on CuO-NPs can block the redox reaction on the surface of CuO-NPs (Fig. 8). The detection range was 0.03–1.5 nM, and the detection limit was 0.01 nM. Gu et al.[107] used CuO@mesoporous carbon (CuOx@mC) which was synthesized by direct pyrolysis of the metal–organic skeleton to construct glyphosate electrochemical sensors. There was strong chelation between the groups (P=O, C=O, N–H) and Cu^{2+}, which can lead to producing a stable glyphosate Cu(II) complex. The mesoporous carbon has an ultra-high porosity and a larger surface area, which provides more active sites for CuO and increases the electron transfer rate, thereby accelerating the reaction of glyphosate and CuO. Tian et al.[108] used a liquid-controlled precipitation method to prepare CuO–TiO_2 and modified it on a GCE for methyl parathion determination. The high active surface area and good biocompatibility of TiO_2 greatly improve the electron transfer capability of the CuO and the electrode. The electrodes show a strong affinity for methyl parathion, inhibiting the redox reaction of CuO and thereby indirectly detecting methyl parathion. In addition, Xie et al.[109] calcined Cu(II)/Ce(III) metal–organic frameworks to prepare nanostructured copper-cerium oxide (CuO–CeO_2) composites for the determination of malathion. The principle of this sensor for malathion detection is also based on the affinity of CuO for malathion. Synergistic interactions between CuO and CeO_2 improve the detection performance.

Furthermore, Ghodsi et al.[59] employed TiO_2 NPs/MWCNTs/ GCE to detect diazinon. MWCNTs/TiO_2NPs which were synthesized by calcination exhibited excellent synergistic electrocatalytic performance in diazinon reduction. Kumaravel et al.[110] covered the surface of a GCE with TiO_2/Nafion, to form a uniform film that was used for the direct detection of fenitrothion. It was found that there is an interaction between TiO_2 and Nafion, because the transition metal Ti tends to form coordination compounds with the sulfur atoms of the sulfonic acid group in Nafion, indicating that the combination of the phosphoric acid group in fenthion and the TiO_2 nanoparticles with carboxyl groups enhances the ability in electron transfer. ReddyPrasad et al.[111] modified carbon dots/zirconium dioxide (C-dots/ZrO_2) on the GCE by electrochemical deposition, to prepare a methyl parathion sensor. Compared with C-dots/GCE and ZrO_2/GCE, C-dots/ZrO_2/GCE showed a better electrochemical response. The reason is that the modified C-dots/ZrO_2 combines the advantages of the large surface area of C-dots and the strong affinity of ZrO_2 for phosphate groups, and the embedding of ZrO_2 on C-dots increases the contact area between the two. Nitroaromatic OPPs exhibit good redox capabilities on the electrode. Ravi et al.[58] electrodeposited α-

© 2023 The Author(s). Published by the Royal Society of Chemistry

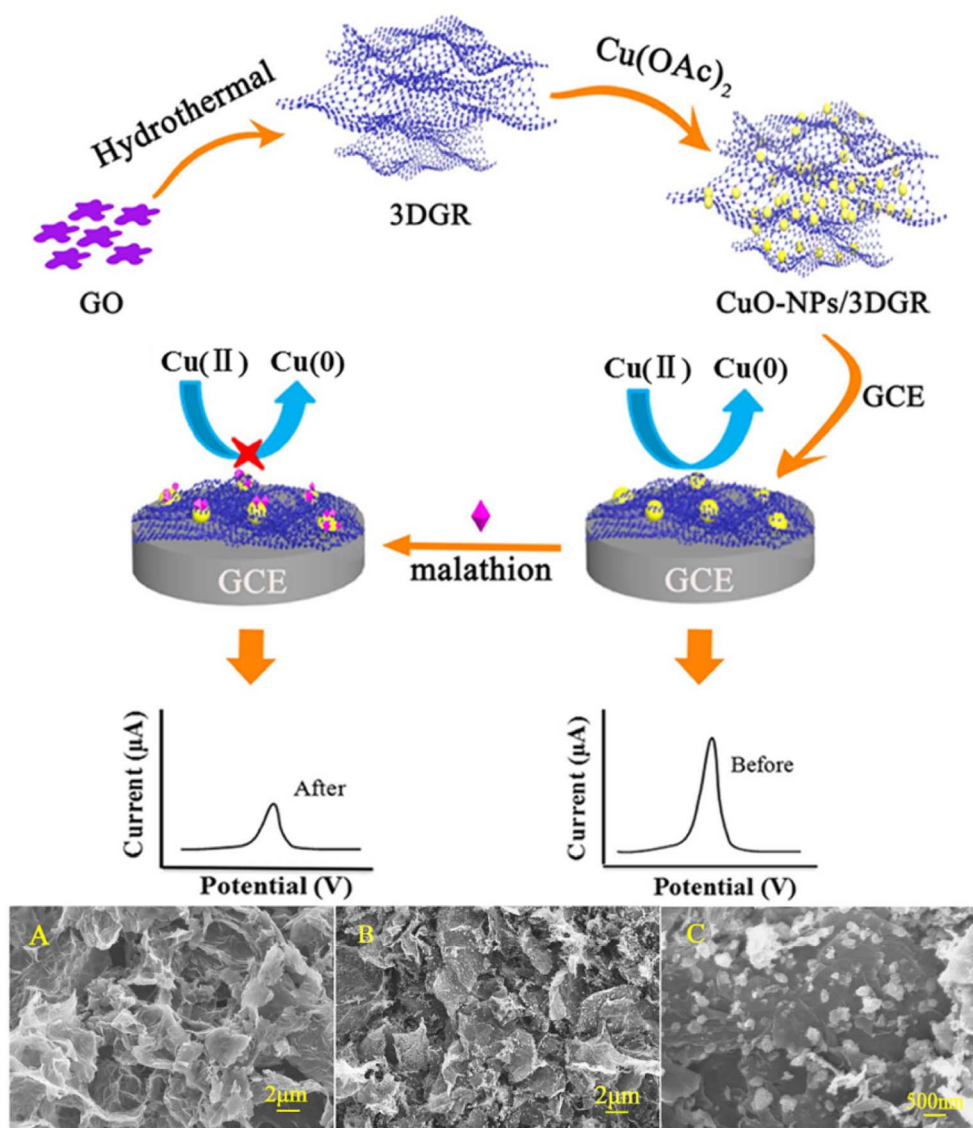*Environ. Sci.: Adv.*, 2023, **2**, 933–956 | **945**

Fig. 8 Scheme of preparation of CuO-NPs/3D GR/GCE and electrochemical detection of malathion; SEM images of 3DGR (A); (B) low- and (C) high-magnification SEM images of the CuO-NPs/3DGR nanocomposite. Reproduced from ref. 53 with permission from Elsevier, copyright 2018.

manganese dioxide nanorods on platinum disc electrodes (MnO_2/Pt) for the detection of 4-nitrophenyl phosphate (4-NPP) which was adsorbed onto electrodes to cause electrochemical reduction. Mn^{2+} ions on the electrode surface, which make it positively charged at neutral pH, help to increase the adsorption rate of OPPs. Rajaji et al.[112] designed a strontium hexaferrite (nanorods) decorated on porous graphitic carbon nitride ($SrFe_{12}O_{19}/g$-C_3N_4/SPCE) sensor for the detection of fenitrothion which generates a reduction reaction on the electrode surface. Hydrothermal synthesis of $SrFe_{12}O_{19}$ nanorods interconnected with g-C_3N_4 improved the electrocatalytic performance of the sensor. Maji et al.[113] investigated a one-step combustion route to synthesize rGO-g-C_3N_4-$MnCo_2O_4$ nanocomposites for the detection of chlorpyrifos directly. The sensor has a large surface area due to rGO-g-C_3N_4 and the excellent electrical conductivity of rGO and the good biocompatibility of $MnCo_2O_4$ nanoparticles give the sensor excellent performance.

Khairy et al.[114] used a hydrothermal method to synthesize macroporous nickel oxide nanoenzymes to directly detect the reduction reaction of parathion, and the large specific surface area and mesoporous network structure of NiO (nickel oxide) nanoenzymes improved the sensitivity of the sensor.

Shown in Table 6 is the relevant information of electrochemical sensors fabricated from the above-mentioned nano metal oxides and their composites. It can be seen that nano metal oxides usually need to be combined with other conductive materials in order to have good electrochemical performance in the detection of OPPs. Some oxides have a high affinity for OPPs containing sulfur and phosphoric acid groups, so they are easy to combine with OPPs. Therefore, the oxidation–reduction reaction of the functional material is hindered on the surface of the electrode. The electrochemical response signal of the OPPs is obtained by calculating the inhibition rate of the electrochemical signal of the material. The nanocomposites can

946 | Environ. Sci.: Adv., 2023, **2**, 933–956

© 2023 The Author(s). Published by the Royal Society of Chemistry

Table 6 Comparison of the electrochemical performance of nanometer metal oxides and their composite modified electrodes for OPP determination

Electrode material	Detection method	Linear range (μM)	LOD (μM)	Accumulation/ adsorption time	Stability	Anti-interference	Preparation difficulty level	OPPs	Ref.
CuO-NPs/3D GR/GCE[a]	DPV	3.0×10^{-5}–1.5×10^{-3}	1.0×10^{-5}	90 s	Good	Excellent	Difficult	Malathion	53
MnO$_2$/Pt[b]	CV	0.1–0.9	1.0×10^{-2}	N/A	N/A	Good	Normal	4-Nitrophenyl phosphate	58
TiO$_2$ NPs/MWCNTs[c]	SWV	1.0×10^{-2}–8.4	3.0×10^{-3}	5 s	Good	N/A	Normal	Diazinon	59
ZnO/Ni-foam[d]	ECL	1.0×10^{-8}–8.5×10^{-3}	9.5×10^{-10}	N/A	Excellent	Excellent	Normal	Chlorpyrifos	65
CuOx@mC/GCE[e]	DPV	1.0×10^{-8}–1.0×10^{3}	7.8×10^{-10}	150 s	Good	Excellent	Difficult	Glyphosate	107
CuO–TiO$_2$/GCE[f]	DPV	0–7.7	4.5×10^{-3}	300 s	Good	Excellent	Normal	Parathion-methyl	108
CeO$_2$–CuO/GCE[g]	DPV	1.0×10^{-5}–0.1	3.3×10^{-6}	120 s	Excellent	Excellent	Normal	Malathion	109
TiO$_2$/Nafion/GCE[h]	DPV	0.2–4.0	8.7×10^{-2}	N/A	N/A	N/A	Easy	Fenitrothion	110
C-dots/ZrO$_2$/GCE[i]	AdSV	7.6×10^{-4}–0.2	2.1×10^{-4}	140 s	Good	Excellent	Normal	Parathion-methyl	111
SrFe$_{12}$O$_{19}$/g-C$_3$N$_4$/SPCE[j]	DPV	5.0×10^{-3}–378.2	1.4	50 s	Excellent	Excellent	Normal	Fenitrothion	112
rGO-g-C$_3$N$_4$-MnCo$_2$O$_4$/GCE[k]	DPV	2.8×10^{-5}–19.0	0.9×10^{-6}	300 s	Excellent	Good	Difficult	Chlorpyrifos	113
NiO-SPE[l]	DPV	0.1–30	2.4×10^{-2}	60 s	N/A	Excellent	Normal	Parathion	114
Fe$_3$O$_4$/MIP/m-GEC[m]	SWV	4.6×10^{-6}–9.2	4.6×10^{-6}	3600 s	N/A	Excellent	Normal	Methyl parathion	146
MIP/Co$_3$O$_4$@MOF-74/cycle4/GCE[n]	DPV	1.0×10^{-5}–1.0×10^{-3}	3.0×10^{-6}	1200 s	Excellent	Excellent	Normal	Fenamiphos	147

[a] CuO-NPs/3D graphene/glassy carbon electrode. [b] α-Manganese dioxide nano-rods/platinum electrode. [c] Titanium dioxide NPs/multi-walled carbon nanotubes/glassy carbon electrode. [d] Zinc oxide/Ni-foam. [e] CuO-coated mesoporous carbon/glassy carbon electrode. [f] Copper oxide–titanium dioxide/glassy carbon electrode. [g] Cerium dioxide–copper oxide/glassy carbon electrode. [h] TiO$_2$/Nafion/glassy carbon electrode. [i] Carbon dots/zirconium dioxide/glassy carbon electrode. [j] Strontium hexaferrite/porous graphitic carbon nitride/screen printing electrode. [k] Reduced graphene oxide–graphitic carbon nitride–manganese cobaltite/glassy carbon electrode. [l] Nickel oxide/screen-printed electrode. [m] Triiron tetraoxide/molecularly imprinted polymers/graphite-epoxy composite. [n] Molecularly imprinted polymers/cobalt tetraoxide-coated metal–organic framework-74/cycle4/glassy carbon electrode.

improve their electrocatalytic performance and electrochemical activity, and greatly reduce the detection limit.

4.4 Conductive nano-polymers and composites

Generally, polymers are not conductive in their neutral state. The conductivity of polymers is produced by charge carriers after doping their conjugated backbone.[115–119] Conductive polymers have the characteristics of flexibility, corrosion resistance, being lightweight, and being of relatively low cost.[120] These unique features make them suitable as replacements for metals and semiconductors. For the application of conductive polymers in various fields, a lot of research has been conducted, such as organic light-emitting diodes,[121,122] energy storage,[123,124] and organic solar cells.[123,125] Recently, conductive polymers have received increasing attention in relation to electrochemical sensors.[126–128] The application of conductive nano-polymers in the detection of OPPs is summarized as follows.

Wu[129] reported the preparation of phoxim sensors with poly(3-methylthiophene)/nitrogen-doped graphene (P3MT/NGE) which was prepared through drop-casting of NGE followed by the electrodeposition of the P3MT film. The synergistic effect of P3MT/NGE can promote electron transfer and charge exchange between the phoxim and the modified electrode surface. Akyüz et al.[130] used solid-state electropolymerization of a film to design a 4-azido-polyaniline/terminal alkyne-substituted manganese phthalocyanine/ITO (indium tin oxide coated glass substrate) sensor, which combines terminal

alkyne-substituted manganese phthalocyanine (MnPc-TA) and 4-azido-polyaniline (N3-PANI), for the detection of fenitrothion, which is catalytically reduced. The metal phthalocyanine has a conjugated structure, stability, and redox activity which gives the sensor outstanding performance. Additionally, a glassy carbon electrode was modified with polazincon by Ensafi et al.[131] and the results showed that there was better electrochemical behaviour of the modified electrode for fenitrothion. The –NO$_2$ functional group of fenitrothion is reduced to the –NHOH functional group. Tümay et al.[132] developed a new electrochemical sensor based on hybrid nanomaterials with electroactive and electropolymerizable groups. This involved modification of ferrocene–thiophene complexes on carbon nanotubes by click chemistry, with synergistic effects increasing the surface area, conductivity and catalytic properties of the electrodes, and the redox reaction of parathion at the electrode surface. Tefera et al.[60] prepared a cobalt nanoparticle-polypyrrole modified glassy carbon electrode (CoNPs/PPy/GCE) for the detection of phoxim by drop-coating cobalt nanoparticles (CoNPs) onto polypyrrole modified glassy carbon electrodes (PPy/GCE) made by electrodeposition. Reduction of phoxim occurred at the electrode surface. Interaction of PPy chains with CoNPs through donor–acceptor bonds increases the electrode surface area and reduces electron transfer resistance.

Migliorini et al.[63] used chemically reduced graphene oxide pairs (CRGO) to modify polyamide 6 (PA6)/polypyrrole (PPy) based polymer electrospun nanofibres for the detection of
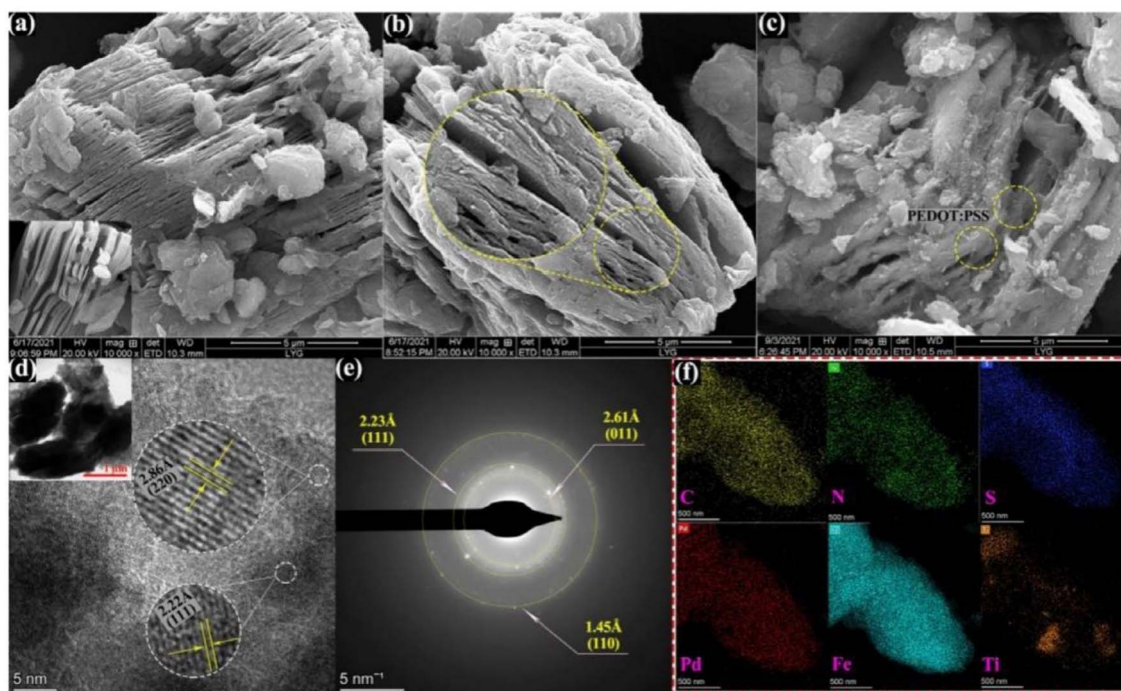
© 2023 The Author(s). Published by the Royal Society of Chemistry

Environ. Sci.: Adv., 2023, **2**, 933–956 | **947**

Fig. 9 SEM images of (a) NS-Ti$_3$C$_2$T$_x$ (inset of pristine-Ti$_3$C$_2$T$_x$), (b) PEDOT:PSS/NS-Ti$_3$C$_2$T$_x$, and (c) Pd–Fe$_3$O$_4$/PEDOT:PSS/NS-Ti$_3$C$_2$T$_x$ composites. (d) TEM and HRTEM image, (e) corresponding SAED pattern, and (f) elemental mappings data of the Pd–Fe$_3$O$_4$/PEDOT:PSS/NS-Ti$_3$C$_2$T$_x$ composite. Reproduced from ref. 133 with permission from Elsevier, copyright 2022.

malathion directly. PPy was mixed with PA6 in a formic acid solution and electrospun nanofibres were obtained by the action of an electrospinning device. The electrospun nanofibres have a large surface area and porosity, and the chemically reduced graphene oxide has good electrical conductivity. These are properties that enhance the performance of the sensor. Recently, Deng *et al.*[133] used Ti$_3$C$_2$T$_x$ for co-doping modification, to synthesize NS-Ti$_3$C$_2$T$_x$. PEDOT:PSS was then inserted between NS-Ti$_3$C$_2$T$_x$ nanospheres as a catalytic carrier for Pd–Fe$_3$O$_4$, leading to the synthesis of a palladium–magnetic iron/poly(3,4-ethylenedioxythiophene):poly(styrene sulfonic acid)/nitrogen and sulfur co-doped titanium carbide (Pd–Fe$_3$O$_4$/PEDOT:PSS/NS-Ti$_3$C$_2$T$_x$) composite framework for the detection of methyl parathion. As shown in Fig. 9 (a–f), the composite has a good composite structure and the elemental components are evenly distributed within, giving the material a good composite state. The sensor exhibits superior catalytic performance in detecting the reduction reaction of methyl parathion. Joshi *et al.*[61] developed polymeric nanocomposites (PNCs) using polyindole-modified stainless steel substrates of tungsten carbide, to increase the conductivity of the sensor and the electron transfer rate for electrochemical detection of chlorpyrifos. This involved promotion of indole polymerization using surfactants followed by deposition of PNCs on tungsten carbide, resulting in a sensor with superior performance for direct redox detection of chlorpyrifos.

In Table 7, we have summarized the non-enzymatic electrochemical sensors, in terms of nano-conductive polymers and nano-composites, for OPP testing. Nano-conductive polymers

have the characteristics of strong conductivity, redox, and stability. When combined with metal nanoparticles, metal compounds, or conductive carbon nanomaterials, the selectivity of the sensor and the electroactive surface area of the electrode were improved. This can make the modified electrode exhibit fast electron transfer kinetics.

4.5 Metal–organic frameworks and composites

Metal–organic framework (MOF) materials are a new class of porous nanomaterials, also known as porous coordination polymers, consisting of a central metal ion and multiple ligands, which have seen tremendous development in the last few decades. Due to their tunable porosity, large specific surface area, open metal sites, and easily modifiable chemical substances, MOFs have been widely used in sensor design.[134] The application of metal–organic frameworks in the detection of OPPs is summarized as follows.

MOFs are mainly formed by the coordination of metal centres and organic ligands to form coordination bonds. At the same time, hydrogen bonding, van der Waals forces, and π–π stacking play an important role in the structure of MOFs. Hu *et al.*[135] combined Fe$_3$O$_4$ (Triiron tetraoxide) nanoparticles with a MOF to form a magnetic metal–organic framework composite by a hydrothermal method. The magnetic properties and superior porosity of the sensor allow it to accumulate methyl parathion, resulting in superior performance in the detection of methyl parathion reduction reactions. Gao *et al.*[136] designed a zirconium-based metal–organic framework material (Zr-BDC) synthesized by a hydrothermal method with terephthalic acid as

Table 7 Comparison of electrochemical performance of nano-conducting polymers and their composite modified electrodes for OPP determination

Electrode material	Detection method	Linear range (µM)	LOD (µM)	Accumulation/ adsorption time	Stability	Anti-interference	Preparation difficulty level	OPPs	Ref.
CoNPs/PPy/GCE[a]	SWV	2.5×10^{-2}–12	4.5×10^{-3}	50 s	Average	Excellent	Normal	Phoxim	60
PIN/WC[b]	SWV	2.5–22.5	5.9×10^{-3}	N/A	N/A	N/A	Normal	Chlorpyrifos	61
PA6/PPy/CRGO/FTO[c]	DPV	1.7–67.1	2.7×10^{-3}	N/A	N/A	Good	Normal	Malathion	63
P3MT/NGE/GCE[d]	CV	2.0×10^{-2}–0.2; 0.2–2.0	6.4×10^{-3}	180 s	N/A	Excellent	Normal	Phoxim	129
N3-PANI/MnPc-TA/ITO[e]	SWV	0.1–15.0	4.9×10^{-2}	N/A	Average	N/A	Normal	Fenitrothion	130
Polyzincon/GCE[f]	DPV	5.0×10^{-3}–8.6	1.5×10^{-3}	175 s	N/A	Excellent	Normal	Fenitrothion	131
FT@CNT/GCE[g]	DPV	2.0×10^{-2}–6.5	5.3×10^{-3}	N/A	Average	Excellent	Normal	Parathion	132
Pd–Fe$_3$O$_4$/PEDOT: PSS/NS-Ti$_3$C$_2$T$_x$/GCE[h]	LSV	1.0×10^{-2}–140.0	3.3×10^{-3}	N/A	Good	Excellent	Difficult	Parathion-methyl	133
ICP@MWNT/GCE[i]	DPV	0.2×10^{-4}–1.0	4.0×10^{-6}	N/A	N/A	Excellent	Normal	Chlorpyrifos	148

[a] Cobalt nanoparticles/polypyrrole/glassy carbon electrode. [b] Polyindole/tungsten carbide. [c] Polyamide 6/polypyrrole/chemically reduced graphene oxide/fluorine tin oxide. [d] Poly(3-methylthiophene)/nitrogen-doped graphene/glassy carbon electrode. [e] 4-Azido polyaniline/terminal alkynyl substituted manganese phthalocyanine/indium tin oxide. [f] Polyzincon/glassy carbon electrode. [g] Ferrocene–thiophene coated carbon nanotube/ glassy carbon electrode. [h] Palladium–magnetic iron/poly(3, 4-ethylenedioxythiophene):poly(styrenesulfonic acid)/nitrogen and sulfur co-doped titanium carbide/glassy carbon electrode. [i] Molecular imprinting with a conducting polythiophene copolymer-coated multiwalled carbon nanotubes/glassy carbon electrode.

the ligand, which was combined with electro-reduced graphene oxide (rGO) to form nanocomposites that not only have a high affinity for methyl parathion, but also have a large specific surface area and favorable electron transport capacity, thus, favoring direct detection of methyl parathion. Karimian et al.[137] constructed sensors based on TiO$_2$-functionalised graphene oxide@UiO-66 (a metal–organic backbone with Zr as the metal centre and terephthalic acid as the organic ligand) (TGO@UiO-66) metal–organic framework composite nanomaterials by a hydrothermal method, for the direct detection of parathion and chlorpyrifos. The glassy carbon electrode was modified with

TGO@UiO-66, which enhances the electron transfer rate and electrocatalytic performance and considerably improves the performance of the sensor. Recently, Janjani et al.[138] investigated the Mn^{2+} (manganese ions)/Fe^{3+} (iron ions) bimetallic organic framework, which modified screen-printed electrodes for the direct detection of chlorpyrifos (Fig. 10). MnFe–MOF was synthesized using a one-pot solution thermal method. Due to the heterometallic synergy between Mn^{2+} and Fe^{3+} ions, both the adsorption and electrocatalytic effect of the sensor on chlorpyrifos were increased.

Fig. 10 Scheme of preparation for MnFe–MOF/SPE and electrochemical detection of chlorpyrifos; PXRD pattern of MnFe–MOF (A); SEM micrograph of MnFe–MOF (B). Reproduced from ref. 138 with permission from Elsevier, copyright 2022.

Table 8 Comparison of electrochemical performance of metal–organic frameworks and their composite modified electrodes for OPP determination

Electrode material	Detection method	Linear range (μM)	LOD (μM)	Accumulation/adsorption time	Stability	Anti-interference	Preparation difficulty level	OPPs	Ref.
Fe$_3$O$_4$/MOF[a]	DPV	1.9×10^{-2}–19.0	1.2×10^{-2}	300 s	N/A	N/A	Normal	Methyl parathion	135
Zr-BDC-rGO/GCE[b]	SWV	1.0×10^{-3}–3.0	0.5×10^{-3}	720 s	Good	Excellent	Difficult	Methyl parathion	136
TGO@UiO-66/GCE[c]	SWV	5.0×10^{-3}–300.0×10^{-3}	1.0×10^{-3}	N/A	Good	Excellent	Normal	Chlorpyrifos	137
MnFe-MOF/SPE[d]	SWV	1.0×10^{-3}–100.0×10^{-3}	0.9×10^{-3}	120 s	N/A	Excellent	Normal	Chlorpyrifos	138
BTCA-P-Cu-CP/CPE[e]	CV	0.6×10^{-3}–24.0×10^{-3}	0.2×10^{-3}	80 s	Excellent	Excellent	Normal	Malathion	139
Cu-TCPP/AuNPs/CP[f]	DPV	0.2–120.0	3.0×10^{-2}	60 s	Good	Good	Normal	Glyphosate	140
Nd-UiO-66@MWCNT/GCE[g]	DPV	0.7×10^{-3}–100.0×10^{-3} 1.0×10^{-3}–120.0×10^{-3}	0.4×10^{-4} 0.7×10^{-4}	N/A	Average	Excellent	Normal	Paraoxon parathion	141
Aptamer-Au NPs @rGO/CdTe QDs@NH2-MIL-88(Fe)/GCE[h]	ECL	3.0×10^{-9}–3.0×10^{-3}	9.1×10^{-10}	N/A	N/A	Excellent	Difficult	Malathion	142
MIP/Co$_3$O$_4$@MOF-74/cycle4/GCE[i]	DPV	1.0×10^{-5}–1.0×10^{-3}	3.0×10^{-6}	1200 s	Excellent	Excellent	Normal	Fenamiphos	147

[a] Triiron tetraoxide/MOF. [b] Zirconium-based metal–organic framework material with terephthalic acid as a ligand/reduced graphene oxide/glassy carbon electrode. [c] TiO$_2$ functionalized graphene oxide coated Universitetet i Oslo metal–organic frameworks/glassy carbon electrode. [d] Bimetallic Mn^{2+}/Fe^{3+} metal–organic framework/screen-printed electrode. [e] Copper-based porous coordination polymer/carbon paste electrode. [f] Copper porphyrin metal–organic framework/gold nanoparticles/carbon paper. [g] Neodymium/Universitetet i Oslo coated multi-walled carbon nanotubes/glassy carbon electrode. [h] Aptamer-gold nanoparticles/reduced graphene oxide/cadmium telluride quantum dots/Fe-based metal–organic framework/glassy carbon electrode. [i] Molecularly imprinted polymer/cobalt tetraoxide coated metal–organic framework-74/cycle4/glassy carbon electrode.

Al'Abr *et al.*[139] used a BTCA-P-Cu-CP (copper-based porous coordination polymer) modified CPE (carbon paste electrode) to detect malathion. The high porosity of BTCA-P-Cu-CP increases the adsorption of malathion and thus affects the redox reaction of CuO. Recently, Jiang *et al.*[140] investigated a non-enzymatic sensor based on Cu-TCPP/AuNPs/CP (modification of carbon paper with copper porphyrin metal–organic frameworks and gold nanoparticles) which was synthesized by a hydrothermal method. The sensor increased the copper sites that could bind to glyphosate, which inhibits the redox reaction of Cu^{2+}, thus improving selectivity and sensitivity. Khoshsafar *et al.*[141] introduced neodymium (Nd) into a Universitetet i Oslo (UiO-66) structure and added multi-walled carbon nanotubes to create a Nd-UiO-66@MWCNT nanocomposite, synthesized by a solvothermal procedure. The high surface area, outstanding stability, and excellent electrocatalytic properties of the sensor facilitate the direct detection of parathion and paraoxon. Chen *et al.*[142] constructed an aptamer-based electrochemiluminescence sensor (aptamer-Au NPs/CdTe (cadmium telluride quantum dots)@rGO QDs@NH_2-MIL-88(Fe)(Fe-based metal–organic framework)/GCE which was synthesized by a hydrothermal method, for the detection of malathion indirectly, in which the iron-based organic framework NH_2-MIL-88(Fe) can be used to enhance the luminescence signal of CdTe QDs, to achieve excellent detection performance. Fe(II) of NH_2-MIL-88(Fe) acts as a signal enhancer, reacting with $S_2O_8^{2-}$ to produce Fe(III) and SO_4^- free radicals, which are reduced under electrochemical reactions, and SO_4^- radicals, which can react with CdTe QDs to give relatively stronger ECL signals.

Most MOF materials are insulators or semiconductors, therefore improving the electrical conductivity of MOFs. Designing MOFs with redox activity is the main challenge for their application in electrochemical detection. The porous properties and large surface area of MOFs allow the incorporation of heterogeneous nanostructured materials, which has facilitated the development of applications based on MOFs. An important direction for MOFs is the exploration of nanomaterial construction of MOFs. The metal–organic frameworks and their composites for the detection of OPPs are shown in Table 8.

4.6 Molecularly imprinted polymers and composites

Molecularly imprinted polymers (MIPs) are polymers that are processed using molecular imprinting techniques. The idea for this technology originated in the field of immunology. Being the technology of polymeric materials with the ability to recognize specific target molecules, MIPs have gained great interest in practical applications, due to their higher physical and chemical stability compared to methods that use antibodies as bioreceptors.[143]

Molecular imprinting, functional monomers, and cross-linking agents are used to form polymers, and under specific conditions, the imprinted molecules are removed, so that the polymers form cavities that can specifically identify the target. Wu *et al.*[55] constructed a non-enzymatic sensor to detect methylparathion through the electropolymerization of *p*-ATP (*p*-aminothiophenol) and FuAuNP (functionalized gold nanoparticles), into which the template molecule was embedded. Gold nanoparticle-modified carbon nanotube nanocomposites (AuNP-MCNT) have been used to improve the effective sites and electrical conductivity of the imprint. Additionally, electropolymerization of pyrrole on gold microelectrodes was done, to construct molecularly imprinted polymer films for chlorpyrifos detection by Napabooshanam *et al.*[144] Molecularly imprinted polymers (MIPs) are synthesized by electrochemical deposition,

Fig. 11 Scheme of preparation for MIP/ZnOHS/GCE and electrochemical detection of methyl parathion. Reproduced from ref. 145 with permission from Elsevier, copyright 2021.

© 2023 The Author(s). Published by the Royal Society of Chemistry

Environ. Sci.: Adv., 2023, **2**, 933–956 | **951**

Environmental Science: Advances

Table 9 Comparison of electrochemical performance of molecularly imprinted polymers and their composite modified electrodes for OPP determination

Electrode material	Detection method	Linear range (μM)	LOD (μM)	Accumulation/ adsorption time	Stability	Anti-interference	Preparation difficulty level	OPPs	Ref.
FuAuNP–ATP–MIP–AuNP–MCNT/GCE[a]	LSV	0.4×10^{-3} –4.2×10^{-2}	0.3×10^{-3}	360 s	Good	Excellent	Difficult	Methyl parathion	55
MIPNs/SPE[b]	DPV	1.5×10^{-2}–2.1	1.2×10^{-2}	300 s	Average	Excellent	Normal	Glyphosate	66
PPy/Au-μE[c]	DPV	1.0×10^{-9}–1.0	0.9×10^{-9}	480 s	Excellent	Excellent	Normal	Chlorpyrifos	144
MIP/ZnOHS/GCE[d]	DPV	5.0×10^{-4}–10.0	5.0×10^{-4}	N/A	Good	Excellent	Normal	Methyl parathion	145
Fe$_3$O$_4$/MIP/m-GEC[e]	SWV	4.6×10^{-6}–9.2	4.6×10^{-6}	3600 s	N/A	Excellent	Normal	Methyl parathion	146
MIP/Co$_3$O$_4$@MOF-74/cycle4/GCE[f]	DPV	1.0×10^{-5} –1.0×10^{-3}	3.0×10^{-6}	1200 s	Excellent	Excellent	Normal	Fenamiphos	147
ICP@MWNT/GCE[g]	DPV	0.2×10^{-4}–1.0	4.0×10^{-6}	N/A	N/A	Excellent	Normal	Chlorpyrifos	148
CuNPs@GR-MIP[h]	DPV	5.0×10^{-2}–50.0	2.4×10^{-4}	720 s	Excellent	Excellent	Normal	Parathion methyl	149
MIP/MoS$_2$NPs@MWCNTs/GCE[i]	DPV	1.0×10^{-5} –1.0×10^{-3}	2.0×10^{-6}	N/A	Excellent	Excellent	Difficult	Paraoxon	150

[a] Functionalized gold nanoparticles-*p*-aminothiophenol-molecularly imprinted polymer – gold nanoparticles–carbon nanotube nanocomposites/glassy carbon electrode. [b] Molecularly imprinted polypyrrole nanotubes/screen-printed electrode. [c] Polypyrrole/gold microelectrodes. [d] Molecularly imprinted polymer/zinc oxide hollow spheres/glassy carbon electrode. [e] Triiron tetraoxide/molecularly imprinted polymer/graphite-epoxy composite. [f] Molecularly imprinted polymer/cobalt tetraoxide coated metal–organic framework-74/cycle4/glassy carbon electrode. [g] Molecular imprinting with a conducting polythiophene copolymer-coated multiwalled carbon nanotubes/glassy carbon electrode. [h] Copper nanoparticles decorated vinyl-functionalized graphene-molecularly imprinted polymer. [i] Molecularly imprinted polymer/molybdenum disulfide nanoparticles/coated multiwalled carbon nanotubes/glassy carbon electrode.

a method that increases the stability of the sensor. Daizy et al.[145] synthesized molecularly imprinted polymer films by electropolymerizing the functional monomer L-arginine (L-Arg) and the template molecule on glassy carbon electrodes modified with zinc oxide (ZnO) hollow spheres (ZnOHS). The sensor selectively detected methyl-parathion and the hollow structure of ZnO provided the sensor with a large surface area and sensitivity (Fig. 11). Ding et al.[66] modified a molecularly imprinted polymer, prepared by embossing glyphosate sites into the surface of polypyrrole nanotubes, onto a screen-printed electrode and assembled it with a 3D-printed electrode holder. The molecularly imprinted polymers for this sensor had high affinity for glyphosate and high electrical conductivity due to nanotubes. Hassan et al.[146] developed a magneto-actuated electrochemical sensor that pre-concentrates pesticides on a magnetic molecularly imprinted polymer. Magnetic molecularly imprinted polymers are synthesized by the magnetic core–shell strategy, and using methacrylic acid as the functional monomer. The sensor showed excellent performance in detecting methyl parathion when compared with a magnetic, non-imprinted polymer sensor.

Additionally, Karimi-Maleh et al.[147] modified glassy carbon electrodes with Co$_3$O$_4$ (cobalt tetraoxide)@MOF-74 nanocomposites (the coordination between divalent transition metals and 2,5-dihydroxyterephthalic acid forms the family of MOF-74 (M: Co, Fe, Ni, Mg, and Mn)), and used pyrrole as monomer and fenamiphos as a template, for molecularly imprinted electrochemical sensors. Co$_3$O$_4$@MOF-74 nanocomposites are prepared by a solvothermal technique which offers high sensitivity and conductivity for sensors. Anirudhan et al.[148] synthesized copolymers of 3-thiophene acetic acid and

3,4-ethylene dioxythiophene on multi-walled carbon nanotubes to improve the conductivity of the sensing device, which is prepared by *in situ* chemical oxidative polymerization, leading to the construction of a molecularly imprinted sensor with good conductivity and a large surface area, that can detect chlorpyrifos. Copper nanoparticles modified on vinyl-functionalized graphene and molecularly imprinted polymers fabricated on them were studied by Sooraj et al.[149] The sensor uses methyl parathion as a template, methacrylic acid as a monomer, and vinyl-functionalized graphene modified with copper nanoparticles, synthesized by reducing propane copper complexes (DAPCu) to increase the performance of the sensor. Bölükbaşı et al.[150] fabricated multi-walled carbon nanotubes (MWCNTs)/molybdenum disulfide nanoparticle (MoS$_2$NP) nanocomposites, which have excellent electron transfer capacity and specific surface area, properties that are of interest, by a hydrothermal method to modify glassy carbon electrodes, and then used parathion as the template and pyrrole as the monomer, to make a molecularly imprinted electrochemical sensor that could detect parathion.

Combining polymer films with nanomaterials provides a large surface area and improves the accessibility of analytes to the identified sites, and the corresponding kinetics. The incorporation of different nanomaterials into MIPs or nano-sized MIPs can combine and enhance the properties of polymeric and inorganic nanomaterials. Nanomaterial-based composites of MIPs offer great analytical potential for improving multi-hybrid MIP systems. The molecularly imprinted polymers and their composites that are used for the detection of OPPs are shown in Table 9.

5. Future perspectives

Herein, we briefly summarize the research progress of non-enzymatic nanomaterials in the electrochemical detection of OPP residues. These developments benefit from the unique physicochemical and electrochemical properties of nanomaterials, which are useful in the creation of electrochemical sensors. In recent years, the uses of carbon nanotubes and graphene have attracted widespread attention, because the high conductivity of these materials can increase the electron transfer rate, thereby enhancing their sensitivity. The combination of various metals and metal compounds with other materials has been continuously explored, owing to their synergistic sensitization effect and excellent electrocatalytic activity. These materials include alloys, metals, and metal oxide composite materials. Polymer-modified composites are used as electrode modification materials, due to their high selectivity and good compatibility. Recent research on nanotechnology has focused on the versatile preparation and application of nanoscale structure construction. Nanostructures with unique properties and specific selectivity have brought innovative development of non-enzymatic OPP sensors. As a matter of fact, enzymatic electrochemical sensors have inherent drawbacks, in that they are easily affected by pH, temperature, and humidity conditions, which spur research and development of nonenzymatic electrochemical OPP sensing alternatives. Most non-enzymatic sensors to detect OPPs are based on functional materials that directly redox OPPs. Other sensors are mainly characterized by the way that they employ metal oxides to specifically bind with the phosphate groups in OPPs, to inhibit the further redox reaction of the material itself, on the electrode. By calculating the inhibition rate of the electrochemical signal of the material, the electrochemical response signal of the OPP pesticide can be obtained.

However, non-enzymatic sensors also have some disadvantages, such as a narrow detection range and poor selectivity for structure-identical OPPs, which may result in the detection of total concentrations of OPPs in complex environments. Therefore, for the design of new nanomaterials that are compatible with nonenzymatic OPP sensors, it is necessary to achieve higher and better sensitivity, selectivity, and stability of electrochemical performance. The following points need to be considered whenever constructing a new non-enzymatic nanomaterial: Firstly, its size and shape should be controlled during synthesis, to generate the best amount of, electrochemically active sites with suitable characteristics. Secondly, the composition, structure and specific reaction of nanomaterials with OPPs need to be a priority, to obtain excellent selectivity. Thirdly, a substrate nanomaterial with higher conductivity, better chemical and mechanical stability, and larger surface area should to fabricated, to improve electrochemical performance. Relevant mechanisms are usually attributed to the synergistic effect among various nanomaterials used on electrodes, but few in-depth studies have been carried out to understand the real physicochemical mechanism. Considering the facts, the development of new non-enzymatic OPP electrochemical sensors still has a long way to go. It is anticipated that

these problems could gradually be solved in the future, so that OPP electrochemical sensors based on non-enzymatic nanomaterials, will provide more convenience to society, and detect OPP residues more conveniently and quickly, reducing the harm of OPPs to the environment and human health.

In addition, there will be more breakthroughs in non-enzymatic electrochemical sensors in the future, which will be constantly evolving in the direction of miniaturization, flexibility, integration, and intelligence, and electrochemical sensors with special properties and advantages such as rapid detection of products in the field and management of unexpected situations will continue to emerge and have practical applications. For example, Raymundo-Pereira et al.[151] explored a wearable electrochemical sensor that is embedded in a glove and can detect multiple types of pesticides simultaneously. Fahimi-Kashani et al.[152] have developed a sensor that uses a smartphone to detect colour changes in a proportional fluorescent probe for rapid in situ detection of methyl parathion. Furthermore, Dhamu et al.[153] designed an electrochemical sensor for field deployable detection of glyphosate in agricultural runoff.

6. Conclusion

OPPs and the residues produced by incomplete degradation, do indeed pose a significant threat to human beings, because of their toxicity. Depending on the standards set by various countries, the maximum limit value of OPPs in vegetables and fruits is at the ppm level. To obtain a lower detection limit, a wider linear range and increased anti-interference capability in complex mechanisms, optimal electrochemical techniques still need to be explored. Most of the authors recognize that electrochemical detection technology is simple, time-saving, and low-cost compared with other detection methods. It is of great importance to create more materials, with excellent performance, based on electrochemical methods. Aimed at the detection of some OPPs, some of the reported research studies have very low detection limits (ppm). For example, BNQDs/GO/GCE was used for simultaneous detection of three analytes (methyl parathion, diazinon, and chlorpyrifos) and CuOx@mC/GCE was used for glyphosate detection. For these pesticides, that have been tested using sensors with low sensitivity, we should focus on commercializing the sensors, to replace complex and expensive detection methods. For other OPPs, the non-enzymatic nanomaterial electrochemical sensor is a potential tool that can employ very sensitive analytical methods, so as to ensure compliance with the maximum limits set by various countries.

Conflicts of interest

There are no conflicts to declare.

Acknowledgements

© 2023 The Author(s). Published by the Royal Society of Chemistry

Environ. Sci.: Adv., 2023, **2**, 933–956 | **953**

References

1 X. L. Pan, F. S. Dong, X. H. Wu, X. U. Jun, X. G. Liu and Y. Q. Zheng, *J. Integr. Agric.*, 2019, **18**, 840–853.

2 W. Aktar, D. Sengupta and A. Chowdhury, *Interdiscip. Toxicol.*, 2009, **2**, 1–12.

3 L. Madianos, E. Skotadis, G. Tsekenis, L. Patsiouras, M. Tsigkourakos and D. Tsoukalas, *Microelectron. Eng.*, 2018, **189**, 39–45.

4 S. A. Nsibande and P. B. C. Forbes, *Anal. Chim. Acta*, 2016, **945**, 9–22.

5 M. Eddleston, N. A. Buckley, P. Eyer and A. H. Dawson, *Lancet*, 2008, **371**, 597–607.

6 P. Kumar, K. H. Kim and A. Deep, *Biosens. Bioelectron.*, 2015, **70**, 469–481.

7 S. Prakash and A. K. Verma, *Indian J. Biol.*, 2020, **7**, 65–69.

8 C. S. Pundir and N. Chauhan, *Anal. Biochem.*, 2012, **429**, 19–31.

9 A. D. Southam, A. Lange, A. Hines, E. M. Hill, Y. Katsu, T. Iguchi, C. R. Tyler and M. R. Viant, *Environ. Sci. Technol.*, 2011, **45**, 3759–3767.

10 R. N. Singh, R. K. Pandey, N. N. Singh and V. K. Das, *World J. Zool.*, 2010, **5**, 183–188.

11 A. Subburaj, P. Jawahar, N. Jayakumar, A. Srinivasan and B. Ahilan, *J. Entomol. Zool.*, 2018, **6**, 103–107.

12 M. Banaee, A. Sureda, A. R. Mirvagefei and K. Ahmadi, *Int. J. Environ. Sci. Technol.*, 2013, **7**, 735–744.

13 J. Aislabie and G. Lloyd-Jones, *Soil Res.*, 1995, **33**, 925–942.

14 K. V. Ragnarsdottir, *J. Geol. Soc. London*, 2000, **157**, 859–876.

15 US Environmental Protection Agency, *Setting Tolerances for Pesticide Residues in Foods*, 2017.

16 NPIC, *International Pesticide Regulations*, 2016.

17 Directive C, *Off. J. Eur. Communities*, 1998, **330**(32), 11–12.

18 M. Motojyuku, T. Saito, K. Akieda, H. Otsuka, I. Yamamoto and S. Inokuchi, *J. Chromatogr. B*, 2008, **875**, 509–514.

19 Y. Hori, M. Fujisawa, K. Shimada and Y. Hirose, *J. Anal. Toxicol.*, 2003, **27**, 162–166.

20 Y. Hori, M. Fujisawa, K. Shimada and Y. Hirose, *J. Anal. Toxicol.*, 2001, **25**, 680–684.

21 G. A. D. Silva, F. Augusto and R. J. Poppi, *J. Chromatogr. A*, 2007, **1138**, 251–261.

22 A. Q. B. Abou-Donia and M. B. Abou-Donia, *J. Pharm. Biomed. Anal.*, 2001, **26**, 291–299.

23 T. Pérez-Ruiz, C. Martínez-Lozano, V. Tomás and J. Martín, *Anal. Chim. Acta*, 2005, **540**, 383–391.

24 J. Bernal, J. L. Bernal, M. T. Martin, M. J. Nozal, A. Anadón, M. R. Martínez-Larraaga and M. A. Martínez, *J. Chromatogr. B*, 2010, **878**, 3290–3296.

25 Y. X. Li, S. J. Zhang, C. H. Song and J. M. You, *Food Anal. Methods*, 2013, **6**, 1284–1290.

26 C. D. Stalikas and C. N. Konidari, *J. Chromatogr. A*, 2001, **907**, 1–19.

27 L. Hou and H. K. Lee, *J. Chromatogr. A*, 2004, **1038**, 37–42.

28 E. Borrás, P. Sánchez, A. Munoz and L. A. Tortajada-Genaro, *Anal. Chim. Acta*, 2011, **699**, 57–65.

29 H. Bagheri, A. Afkhami, H. Khoshsafar, A. Hajian and A. Shahriyari, *Biosens. Bioelectron.*, 2017, **89**, 829–836.

30 G. L. Qian, L. M. Wang, Y. R. Wu, Q. Zhang, Q. Sun, Y. Liu and F. Q. Liu, *Food Chem.*, 2009, **117**, 364–370.

31 E. A. Songa and J. O. Okonkwo, *Talanta*, 2016, **155**, 289–304.

32 Y. Z. Wang, H. X. Qiu, S. Q. Hu and J. H. Xu, *Sens. Actuators, B*, 2010, **147**, 587–592.

33 L. Svorc, M. Rievaj and D. Bustin, *Sens. Actuators, B*, 2013, **181**, 294–300.

34 M. Khairy, H. A. Ayoub and C. E. Banks, *Food Chem.*, 2018, **255**, 104–111.

35 R. T. Paschoalin, N. O. Gomes, G. F. Almeida, S. Bilatto, C. S. Farinas, S. A. Machado, L. H. Mattoso, O. N. liveiraJr and P. A. Raymundo-Pereira, *Biosens. Bioelectron.*, 2022, **199**, 113875.

36 P. A. Raymundo-Pereira, N. O. Gomes, J. H. Carvalho, S. A. Machado, O. N. Oliveira Jr and B. C. Janegitz, *ChemElectroChem*, 2020, **7**, 3074–3081.

37 K. Wang, Q. Liu, L. Dai, J. J. Yan, C. Ju, B. J. Qiu and X. Y. Wu, *Anal. Chim. Acta*, 2011, **695**, 84–88.

38 J. Wang and M. Musameh, *Anal. Chem.*, 2003, **75**, 2075–2079.

39 C. Sahub, T. Tuntulani, T. Nhujak and B. Tomapatanaget, *Sens. Actuators, B*, 2018, **258**, 88–97.

40 E. Mahmoudi, H. Fakhri, A. Hajian, A. Afkhami and H. Bagheri, *Bioelectrochemistry*, 2019, **130**, 107348.

41 G. Yu, W. Wu, Q. Zhao, X. Wei and Q. Lu, *Biosens. Bioelectron.*, 2015, **68**, 288–294.

42 P. Hashemi, N. Karimian, H. Khoshsafar, F. Arduini, M. Mesri, A. Afkhami and H. Bagheri, *Mater. Sci. Eng., C*, 2019, **102**, 764–772.

43 K. E. Toghill and R. G. Compton, *Int. J. Electrochem. Sci.*, 2010, **5**, 1246–1301.

44 N. Gao, C. He, M. Ma, Z. Cai, Y. Zhou, G. Chang and Y. He, *Anal. Chim. Acta*, 2019, **1072**, 25–34.

45 S. Viswanathan and P. Manisankar, *J. Nanosci. Nanotechnol.*, 2015, **15**, 6914–6923.

46 Z. Chen, Y. Zhang, Y. Yang, X. Shi, L. Zhang and G. Jia, *Sens. Actuators, B*, 2021, **336**, 129721.

47 H. Fu, P. Tan, R. Wang, S. Li, H. Liu, Y. Yang and Z. Wu, *J. Hazard. Mater.*, 2022, **424**, 127494.

48 L. G. Sultatos, *J. Toxicol. Environ. Health Part A*, 1994, **43**, 271–289.

49 D. L. Bull, *Residue Rev.*, 1972, **43**, 1–22.

50 J. U. N. Tang, R. L. Rose and J. E. Chambers, *Metabolism of organophosphorus and carbamate pesticides*, Academic Press, Burlington, 1st edn, 2006.

51 D. G. Karpouzas and B. K. Singh, *Adv. Microb. Physiol.*, 2006, **51**, 119–225.

52 V. Velusamy, S. Palanisamy, S. W. Chen, S. Balu, T. C. Yang and C. E. Banks, *Talanta*, 2019, **192**, 471–477.

53 Y. Xie, Y. H. Yu, L. M. Lu, X. Ma, L. Gong, X. G. Huang, G. B. Liu and Y. F. Yu, *J. Electroanal. Chem.*, 2018, **812**, 82–89.

54 M. A. Kamyabi and M. Moharramnezhad, *Microchem. J.*, 2022, **179**, 107421.

55 B. Wu, L. Hou, M. Du, T. Zhang, Z. Wang, Z. Xue and X. Lu, *RSC Adv.*, 2014, **4**, 53701–53710.

56 L. M. Wang, J. B. Dong, Y. L. Wang, Q. Cheng, M. M. Yang, J. Cai and F. Q. Liu, *Sci. Rep.*, 2016, **6**, 1–8.

57 P. Balasubramanian, T. S. T. Balamurugan, S. M. Chen, T. W. Chen, G. Sharmila and M. C. Yu, *J. Taiwan Inst. Chem. Eng.*, 2018, **87**, 83–90.

58 A. K. Ravi, N. Punnakkal, S. P. Vasu, B. G. Nair and S. B. TG, *J. Electroanal. Chem.*, 2020, **859**, 113841.

59 J. Ghodsi and A. A. Rafati, *J. Electroanal. Chem.*, 2017, **807**, 1–9.

60 M. Tefera, M. Tessema, S. Admassie, M. Ward, L. Phelane, E. I. Iwuoha and P. G. Baker, *Anal. Chim. Acta: X*, 2021, **9**, 100077.

61 P. Joshi, S. Mehtab, M. G. H. Zaidi, T. Tyagi and A. Bisht, *J. Nanostruct. Chem.*, 2020, **10**, 33–45.

62 L. Yan, X. R. Yan, H. L. Li, X. F. Zhang, M. Wang, S. F. Fu, G. T. Zhang, C. Qian, H. Y. Yang, J. Y. Han and F. J. Xiao, *Microchem. J.*, 2020, **157**, 105016.

63 F. L. Migliorini, R. C. Sanfelice, L. A. Mercante, M. H. Facure and D. S. Correa, *Mater. Res. Express*, 2019, **7**, 015601.

64 Y. Bakytkarim, S. Tursynbolat, J. Huang and L. Wang, *ChemistrySelect*, 2021, **6**, 4056–4062.

65 M. A. Kamyabi and M. Moharramnezhad, *J. Electroanal. Chem.*, 2020, **865**, 114120.

66 S. Ding, Z. Lyu, S. Li, X. Ruan, M. Fei, Y. Zhou and Y. Lin, *Biosens. Bioelectron.*, 2021, **191**, 113434.

67 D. Yu, E. Nagelli, F. Du and L. M. Dai, *J. Phys. Chem. Lett.*, 2010, **1**, 2165–2173.

68 Z. P. Wu, Y. L. Wang, X. B. Liu, C. Lv and Y. S. Li, *Adv. Mater.*, 2019, **31**, 1800716.

69 D. Huo, Q. Li, Y. Zhang, C. Hou and Y. Lei, *Sens. Actuators, B*, 2014, **199**, 410–417.

70 Q. G. He, J. Liu, Y. H. Xia, D. Tuo, P. H. Deng, Y. L. Tian, Y. Y. Wu, G. L. Li and D. C. Chen, *J. Electroanal. Chem.*, 2019, **166**, B805.

71 G. L. Li, J. T. Wu, H. G. Jin, Y. H. Xia, J. Liu, Q. G. He and D. C. Chen, *Nanomaterials*, 2020, **10**, 307.

72 Q. G. He, J. Liu, J. X. Feng, Y. Y. Wu, Y. L. Tian, G. L. Li and D. C. Chen, *Nanomaterials*, 2020, **10**, 125.

73 Y. L. Tian, P. H. Deng, Y. Y. Wu, J. H. Li, J. Liu, G. L. Li and Q. G. He, *J. Electrochem. Soc.*, 2020, **167**, 046514.

74 Y. L. Tian, P. H. Deng, Y. Y. Wu, J. H. Li, J. Liu, G. L. Li and Q. G. He, *Microchem. J.*, 2020, **157**, 104885.

75 S. Liu and X. Guo, *NPG Asia Mater.*, 2012, **4**, e23.

76 Y. Huang and X. Chen, *Nano LIFE*, 2014, **4**, 1441006.

77 L. J. Brennan and Y. K. Gun'ko, *Organometallics*, 2015, **34**, 2086–2097.

78 L. Yang, S. Q. Wang, S. Q. Peng, H. M. Jiang, Y. M. Zhang, W. F. Deng, Y. M. Tan, M. Ma and Q. J Xie, *Chem. Eur. J.*, 2015, **21**, 10634–10638.

79 C. X. Guo and C. M. Li, *Energy Environ. Sci.*, 2011, **4**, 4504–4507.

80 L. T. Le, M. H. Ervin, H. Qiu, B. E. Fuchs and W. Y. Lee, *Electrochem. Commun.*, 2011, **3**, 355–358.

81 H. Tang, J. Zhang, Y. J. Zhang, Q. Q. Xiong, Y. Y. Tong, Y. Li, X. L. Wang, C. D. Gu and J. P. Tu, *J. Power Sources*, 2015, **286**, 431–437.

82 C. Gong, Y. Zhang, M. Yao, Y. Wei, Q. Li, B. Liu and B. Liu, *RSC Adv.*, 2015, **5**, 39746–39751.

83 B. Tang, G. X. Hu, H. Y. Gao and Z. X. Shi, *J. Power Sources*, 2013, **234**, 60–68.

84 Y. Y. Wu, P. H. Deng, Y. L. Tian, J. X. Feng, J. Y. Xiao, J. H. Li, J. Liu, G. L. Li and Q. G. He, *J. Nanobiotechnol.*, 2020, **18**, 1–13.

85 J. Liu, L. L. Sun, G. L. Li, J. Hu and Q. G. He, *Mater. Res. Bull.*, 2021, **133**, 111050.

86 J. X. Feng, P. H. Deng, J. X. Xiao, J. H. Li, Y. L. Tian, Y. Y. Wu, J. Liu, G. L. Li and Q. G. He, *J. Food Compos. Anal.*, 2021, **96**, 103708.

87 F. Magesa, Y. Y. Wu, S. Dong, Y. L. Tian, G. L. Li, J. M. Vianney, J. Buza, J. Liu and Q. G. He, *Biomolecules*, 2020, **10**, 110.

88 P. H. Deng, J. X. Feng, J. Y. Xiao, J. Liu, X. Nie, J. H. Li and Q. G. He, *J. Electrochem. Soc.*, 2020, **167**, 146511.

89 P. H. Deng, X. Nie, Y. Y. Wu, Y. L. Tian, J. H. Li and Q. G. He, *Microchem. J.*, 2021, **160**, 105744.

90 B. W. Wu, L. X. Xiao, M. J. Zhang, C. Yang, Q. Li, G. L. Li, Q. G. He and J. Liu, *J. Solid State Chem.*, 2021, **296**, 122023.

91 P. H. Deng, J. Y. Xiao, J. X. Feng, Y. L. Tian, Y. Y. Wu, J. H. Li and Q. G. He, *Microchem. J.*, 2021, **165**, 106106.

92 H. X. Wu, D. Q. Huo, Y. N. Zhao, A. N. Munmun, J. Z. Hou, L. Miao, C. H. Shen and C. J. Hou, *Sens. Actuators, B*, 2017, **252**, 1118–1124.

93 M. L. Yola, *J. Mol. Liq.*, 2019, **277**, 50–57.

94 U. Rajaji, K. Murugan, S. M. Chen and M. Govindasamy, *Composites, Part B*, 2019, **160**, 268–276.

95 S. Iijima, *Nature*, 1991, **354**, 56–58.

96 Y. Y. Wu, P. H. Deng, Y. L. Tian, Z. Y. Ding, G. L. Li, J. Liu, Z. Zuberi and Q. G. He, *Bioelectrochemistry*, 2020, **131**, 107393.

97 M. Baghayeri, A. Amiri and S. Farhadi, *Sens. Actuators, B*, 2016, **225**, 354–362.

98 S. Y. Zhu, H. J. Li, W. X. Niu and G. B. Xu, *Biosens. Bioelectron.*, 2009, **25**, 940–943.

99 H. Salehzadeh, M. Ebrahimi, D. Nematollahi and A. A. Salarian, *J. Electroanal. Chem.*, 2016, **767**, 188–194.

100 J. Dong, X. D. Wang, F. M. Qiao, P. Liu and S. Y. Ai, *Sens. Actuators, B*, 2013, **186**, 774–780.

101 K. dos Santos Caetano, D. S. da Rosa, T. M. Pizzolato, P. A. M. dos Santos, R. Hinrichs, E. V. Benvenutti and T. M. H. Costa, *Microporous Mesoporous Mater.*, 2020, **309**, 110583.

102 X. Y. Gao, Y. Gao, C. C. Bian, H. Ma and H. L. Liu, *Electrochim. Acta*, 2019, **310**, 78–85.

© 2023 The Author(s). Published by the Royal Society of Chemistry

Environ. Sci.: Adv., 2023, **2**, 933–956 | **955**

103 J. M. Gong, X. J. Miao, T. Zhou and L. Z. Zhang, *Talanta*, 2011, **85**, 1344–1349.

104 V. Renganathan, R. Balaji, S. M. Chen and T. Kokulnathan, *Sens. Actuators, B*, 2020, **307**, 127586.

105 B. Huang, W. D. Zhang, C. H. Chen and Y. X. Yu, *Mikrochim. Acta*, 2010, **171**, 57–62.

106 N. Y. Sreedhar, M. S. Kumar and K. Krishnaveni, *Sens. Actuators, B*, 2015, **210**, 475–482.

107 C. Gu, Q. Wang, L. Zhang, P. Yang, Y. Xie and J. Fei, *Sens. Actuators, B*, 2020, **305**, 127478.

108 X. K. Tian, L. Liu, Y. Li, C. Yang, Z. X. Zhou, Y. L. Nie and Y. X. Wang, *Sens. Actuators, B*, 2018, **256**, 135–142.

109 Y. Xie, X. Tu, X. Ma, Q. Fang, G. Liu, R. Dai and X. Huang, *Mikrochim. Acta*, 2019, **186**, 1–9.

110 A. Kumaravel and M. Chandrasekaran, *J. Electroanal. Chem.*, 2011, **650**, 163–170.

111 P. ReddyPrasad, E. B. Naidoo and N. Y. Sreedhar, *Arabian J. Chem.*, 2019, **12**, 2300–2309.

112 U. Rajaji, S. Chinnapaiyan, T. W. Chen, S. M. Chen, G. Mani, V. Mani and M. S. El-Shikh, *Electrochim. Acta*, 2021, **371**, 137756.

113 B. Maji, L. S. K. Achary, B. Barik, S. J. Sahoo, A. Mohanty and P. Dash, *J. Electroanal. Chem.*, 2022, **909**, 116115.

114 M. Khairy, H. A. Ayoub and C. E. Banks, *Food Chem.*, 2018, **255**, 104–111.

115 J. Pecherz and M. Kryszewski, *Macromol. Chem. Phys.*, 1989, **190**, 865–874.

116 H. C. F. Martens, I. N. Hulea, I. Romijn, H. B. Brom and M. A. J. Michels, *Phys. Rev. B: Condens. Matter Mater. Phys.*, 2003, **67**, 121203.

117 A. Kokil, I. Shiyanovskaya, K. D. Singer and C. Weder, *J. Am. Chem. Soc.*, 2002, **124**, 9978–9979.

118 U. Lange, N. V. Roznyatovskaya and V. M. Mirsky, *Anal. Chim. Acta*, 2008, **614**, 1–26.

119 M. H. Naveen, N. G. Gurudatt and Y. B. Shim, *Appl. Mater. Today*, 2017, **9**, 419–433.

120 J. R. Reynolds, B. C. Thompson and T. A. Skotheim, *Handbook of Conducting Polymers*, CRC Press, Boca Raton, 4th edn, 2019.

121 G. Gustafsson, Y. Cao, G. M. Treacy, F. Klavetter, N. Colaneri and A. J. Heeger, *Nature*, 1992, **357**, 477–479.

122 W. H. Kim, A. J. Mäkinen, N. Nikolov, R. Shashidhar, H. Kim and Z. H. Kafafi, *Appl. Phys. Lett.*, 2002, **80**, 3844–3846.

123 K. Gurunathan, A. V. Murugan, R. Marimuthu, U. P. Mulik and D. P. Amalnerkar, *Mater. Chem. Phys.*, 1999, **6**, 173–191.

124 L. Pan, H. Qiu, C. M. Dou, Y. Li, L. Pu, J. B. Xu and Y. Shi, *Int. J. Mol. Sci.*, 2010, **11**, 2636–2657.

125 T. N. Murakami and M. Grätzel, *Inorg. Chim. Acta*, 2008, **361**, 572–580.

126 M. Gerard, A. Chaubey and B. D. Malhotra, *Biosens. Bioelectron.*, 2002, **17**, 345–359.

127 B. D. Malhotra, A. Chaubey and S. P. Singh, *Anal. Chim. Acta*, 2006, **578**, 59–74.

128 D. G. Pijanowska, A. Kossakowska and W. Torbicz, *Biocybern. Biomed. Eng.*, 2011, **31**, 43–57.

129 L. H. Wu, W. Lei, Z. Han, Y. H. Zhang, M. Z. Xia and Q. L. Hao, *Sens. Actuators, B*, 2015, **206**, 495–501.

130 D. Akyüz and A. Koca, *Sens. Actuators, B*, 2019, **283**, 848–856.

131 A. A. Ensafi, F. Rezaloo and B. Rezaei, *Electroanalysis*, 2017, **29**, 2839–2846.

132 S. O. Tümay, A. Şenocak, E. Sarı, V. Şanko, M. Durmuş and E. Demirbas, *Sens. Actuators, B*, 2021, **345**, 130344.

133 L. Deng, J. Yuan, S. Xie, H. Huang, R. Yue and J. Xu, *Electrochim. Acta*, 2022, **407**, 139897.

134 L. Liu, Y. Zhou, S. Liu and M. Xu, *ChemElectroChem*, 2018, **5**, 6–19.

135 L. P. Hu, N. Wu, J. Zheng, J. L. Xu, M. Zhang and P. G. He, *Anal. Sci.*, 2014, **30**, 663–668.

136 N. Gao, R. Tan, Z. Cai, H. Zhao, G. Chang and Y. He, *J. Mater. Sci.*, 2021, **56**, 19060–19074.

137 N. Karimian, H. Fakhri, S. Amidi, A. Hajian, F. Arduini and H. Bagheri, *New J. Chem.*, 2019, **43**, 2600–2609.

138 P. Janjani, U. Bhardwaj, R. Gupta and H. S. Kushwaha, *Anal. Chim. Acta*, 2022, **1202**, 339676.

139 A. M. Al'Abri, S. N. Abdul Halim, N. K. Abu Bakar, S. M. Saharin, B. Sherino, H. Rashidi Nodeh and S. Mohamad, *J. Environ. Sci. Health., Part B*, 2019, **54**, 930–941.

140 R. Jiang, Y. H. Pang, Q. Y. Yang, C. Q. Wan and X. F. Shen, *Sens. Actuators, B*, 2022, **358**, 131492.

141 H. Khoshsafar, N. Karimian, T. A. Nguyen, H. Fakhri, A. Khanmohammadi, A. Hajian and H. Bagheri, *Chemosphere*, 2022, **292**, 133440.

142 P. Chen, Z. Liu, J. Liu, H. Liu, W. Bian, D. Tian and C. Zhou, *Electrochim. Acta*, 2020, **354**, 136644.

143 M. Mahmoudpour, M. Torbati, M. M. Mousavi, M. de la Guardia and J. E. N. Dolatabadi, *TrAC, Trends Anal. Chem.*, 2020, **129**, 115943.

144 S. Nagabooshanam, S. Roy, S. Deshmukh, S. Wadhwa, I. Sulania, A. Mathur and S. S. Roy, *ACS Omega*, 2020, **5**, 31765–31773.

145 M. Daizy, M. R. Ali, M. S. Bacchu, M. A. S. Aly and M. Z. H. Khan, *Environ. Technol. Innovation*, 2021, **24**, 101847.

146 A. H. Hassan, S. L. Moura, F. H. Ali, W. A. Moselhy, M. D. P. T. Sotomayor and M. I. Pividori, *Biosens. Bioelectron.*, 2018, **118**, 181–187.

147 H. Karimi-Maleh, M. L. Yola, N. Atar, Y. Orooji, F. Karimi, P. S. Kumar and M. A. Baghayeri, *J. Colloid Interface Sci.*, 2021, **592**, 174–185.

148 T. S. Anirudhan, V. S. Athira and S. S. Nair, *Food Chem.*, 2022, **381**, 132010.

149 M. P. Sooraj and B. Mathew, *Food Anal. Methods*, 2019, **12**, 1028–1039.

150 Ö. S. Bölükbaşı, B. B. Yola, H. Boyacıoğlu and M. L. Yola, *Food Chem. Toxicol.*, 2022, **163**, 112994.

151 P. A. Raymundo-Pereira, N. O. Gomes, F. M. Shimizu, S. A. Machado and O. N. Oliveira Jr, *Chem. Eng. J.*, 2021, **408**, 127279.

152 N. Fahimi-Kashani and M. R. Hormozi-Nezhad, *Sens. Actuators, B*, 2020, **322**, 128580.

153 V. N. Dhamu and S. Prasad, *Biosens. Bioelectron.*, 2020, **170**, 112609.